Title :

ORCHIDEE MICT-LEAK (r5459), a global model for the production, transport and transformation of dissolved organic carbon from Arctic permafrost regions, Part 1: Rationale, model description and simulation protocol.

Authors:

S.P.K. Bowring[1], R. Lauerwald[2], B. Guenet[1], D. Zhu[1], M. Guimberteau[1,3], A. Tootchi[3], A. Ducharne[3], P. Ciais[1]

Affiliations:

[1] Laboratoire des Sciences du Climat et de l'Environnement, LSCE, CEA, CNRS, UVSQ, 91191 Gif Sur Yvette, France

[2] Department of Geoscience, Environment & Society, Université Libre de Bruxelles, 1050 Bruxelles, Belgium

[3] Sorbonne Université, CNRS, EPHE, Milieux environnementaux, transferts et interaction dans les hydrosystèmes et les sols, Metis, 75005 Paris, France

Abstract

Few Earth System models adequately represent the unique permafrost soil biogeochemistry and its respective processes; this significantly contributes to uncertainty in estimating their responses, and that of the planet at large, to warming. Likewise, the riverine component of what is known as the 'boundless carbon cycle' is seldom recognised in Earth System modelling. Hydrological mobilisation of organic material from a ~1330–1580 PgC carbon stock to the river network results either in sedimentary settling or atmospheric 'evasion', processes widely expected to increase with amplified Arctic climate warming. Here, the production, transport and atmospheric release of dissolved organic carbon (DOC) from high-latitude permafrost soils into inland waters and the ocean is explicitly represented for the first time in the land surface component (ORCHIDEE) of a CMIP6 global climate model (Institut Pierre Simon Laplace (IPSL)). The model, ORCHIDEE MICT-LEAK, which represents the merger of previously described ORCHIDEE versions -MICT and -LEAK, mechanistically represents (a) vegetation and soil physical processes for high latitude snow, ice and soil phenomena, and (b) the cycling of DOC and CO_2, including atmospheric evasion, along the terrestrial-aquatic continuum from soils through the river network to the coast, at 0.5° to 2° resolution. This paper, the first in a two-part study, presents the rationale for including these processes in a high latitude specific land surface model, then describes the model with a focus on novel process implementations, followed by a summary of the model configuration and simulation protocol. The results of these simulation runs, conducted for the Lena River basin, are evaluated against observational data in the second part of this study.

1 Introduction

High-latitude permafrost soils contain large stores of frozen, often ancient and relatively reactive carbon up to depths of over 30m. Soil warming caused by contemporary anthropogenic climate change can be expected to destabilise these stores (Schuur et al., 2015) via microbial or hydrological mobilisation following spring/summer thaw and riverine discharge (Vonk et al., 2015a) as the boundary between discontinuous and continuous permafrost migrates poleward and toward the continental interior over

time. The high latitude soil carbon reservoir may amount to ~1330–1580 PgC (Hugelius et al., 2013, 2014; Tarnocai et al., 2009) –over double that stored in the contemporary atmosphere, while the yearly lateral flux of carbon from soils to running waters may amount to about a fifth of net ecosystem carbon exchange (~400 TgC yr^{-1}), about ~40% of which may be contributed by DOC (McGuire et al., 2009). Excluding the dissolved inorganic carbon and soil CO_2 input components of the total riverine carbon flux, the vast majority (85%) of riverine organic carbon transfer to the Arctic Ocean occurs as dissolved organic carbon (DOC), as described in (e.g.) Suzuki et al. (2006)..

The fact that, to our knowledge, no existing land surface models are able to adequately simultaneously represent this unique high latitude permafrost soil environment, the transformation of soil organic carbon (SOC) to its eroded particulate and DOC forms and their subsequent lateral transport, as well as the response of all these to warming, entails significant additional uncertainty in projecting global-scale biogeochemical responses to human-induced environmental change.

Fundamental to these efforts is the ability to predict the medium under which carbon transformation will occur: in the soil, streams, rivers or sea, and under what metabolising conditions –since these will determine the process mix that will ultimately enable either terrestrial redeposition and retention, ocean transfer, or atmospheric release of permafrost-derived organic carbon. In the permafrost context, this implies being able to accurately represent (i) the source, reactivity and transformation of released organic matter, and; (ii) the dynamic response of hydrological processes to warming, since water phase determines carbon, heat, and soil moisture availability for metabolisation and lateral transport.

For this purpose, we take a specific version of the terrestrial component of the Institut Pierre Simon Laplace (IPSL) global Earth System model (ESM) ORCHIDEE (Organising Carbon and Hydrology In Dynamic Ecosystems), one that is specifically coded for, calibrated with and evaluated on high latitude phenomena and permafrost processes, called ORCHIDEE-MICT (where MICT stands for aMeliorated Interactions between Carbon and Temperature (Guimberteau et al., 2018)). This code is then adapted to include DOC production in the soil (ORCHIDEE-SOM, (Camino-Serrano et al., 2018)), 'priming' of SOC (ORCHIDEE-PRIM,(Guenet et al., 2016, 2018)) and the riverine transport of DOC and CO_2, including in-stream transformations, carbon and water exchanges with wetland soils and gaseous exchange between river surfaces and the atmosphere (ORCHILEAK (Lauerwald et al., 2017), where the suffix 'LEAK' holds no acronym, and refers to the 'leakage' of carbon from terrestrial to aquatic realms).

The resulting model, dubbed ORCHIDEE MICT-LEAK, hereafter referred to as MICT-L for brevity, is therefore able to represent: (a) Permafrost soil and snow physics, thermodynamics to a depth of 38m and dynamic soil hydrology to a depth of 2m; (b) Improved representation of biotic stress response to cold, heat and moisture in high latitudes; (c) Explicit representation of the active layer and frozen-soil hydrologic barriers; buildup of soil carbon stocks via primary production and vertical translocation (turbation) of SOC and DOC; (d) DOC leaching from tree canopies, atmospheric deposition, litter and soil organic matter, its adsorption/desorption to/from soil particles, its transport and transformation to dissolved CO_2 ($CO^*_{2(aq.)}$) and atmospheric release, as well as the production and hydrological transport of plant root-zone derived

Simon Bowring 3/7/y 08:49
Supprimé: Excluding the

Simon Bowring 3/7/y 08:48
Supprimé: dissolved inorganic carbon component of this flux, as well as dissolved CO_2 input from soils

dissolved CO_2; (e) Improved representation of C cycling on floodplains; (f) Priming of organic matter in the soil column and subsequent decomposition dynamics. In combination, these model properties allow us to explore the possibility of reproducing important emergent phenomena observed in recent empirical studies (Fig. 1) arising from the interaction of a broad combination of different processes and factors.

To our knowledge very few attempts have been made at the global scale of modelling DOC production and lateral transfer from the permafrost region that explicitly accounts for such a broad range of high latitude–specific processes, which in turn allows us to match and evaluate simulation outputs with specific observed processes, enhancing our ability to interpret the output from theses models and improve our understanding of the processes represented. The only other attempt at doing so is a Pan-Arctic modelling study by Kicklighter et al. (2013), which is based on a relatively simplified scheme for soil, water and biology. The following segment briefly overviews the dynamics, emergent properties and their overall significance across scales, of permafrost region river basins.

A giant, reactive, fast-draining funnel: A permafrost basin overview

Permafrost has a profound impact on Arctic river hydrology. In permafrost regions, a permanently frozen soil layer acts as a 'cap' on ground water flow (see 'permafrost barrier', right hand side of Fig. 1). This implies that: (i) Near-surface runoff becomes by far the dominant flowpath draining permafrost watersheds (Ye et al., 2009), as shown in Fig. 1d; (ii) The seasonal amplitude of river discharge, expressed by the ratio of maximum to minimum discharge ($Q_{max:min}$ in Fig. 1), over continuous versus discontinuous permafrost catchments is higher as a result of the permafrost barrier; (iii) This concentration of water volume near the surface causes intense leaching of DOC from litter and relevant unfrozen soil layers (Fig. 1g, 1d, e.g. Suzuki et al., (2006) Drake et al., (2015) ; Spencer et al., (2015); (Vonk et al., (2015a,b)); (iv) Permafrost SOC stocks beneath the active layer are physically and thermally shielded from aquatic mobilisation and metabolisation, respectively (Fig. 1g).

Rapid melting of snow and soil or river ice during spring freshet (May-June) drives intensely seasonal discharge, with peaks often two orders of magnitude (e.g. Van Vliet et al., (2012)) above baseflow rates (Fig. 1d). These events are the cause of four, largely synchronous processes: (i) Biogenic matter is rapidly transported from elevated headwater catchments (Fig. 1, right hand side) (McClelland et al., 2016); (ii) Plant material at the soil surface is intensely leached, with subsequent mobilisation and transformation of this dissolved matter via inland waters (Fig. 1d,b,j); During spring freshet, riverine DOC concentrations increase and bulk annual marine DOC exports are dominated by the terrestrial DOC flux to the rivers that occurs at this time (Holmes et al., 2012). Indeed, DOC concentrations during the thawing season tend to be greater than or equal to those in the Amazon particularly in the flatter Eurasian rivers (Holmes et al., 2012; McClelland et al., 2012), and DOC concentrations are affected at watershed scale by parent material, ground ice content (O'Donnell et al., 2016) and active layer depth (Suzuki et al., 2006).

(iii) Sudden inundation of the floodplain regions in spring and early summer (Fig. 1h), (Smith and Pavelsky, 2008), further spurs lateral flux of both particulate and dissolved

matter in the process and its re-deposition (Zubrzycki et al., 2013) or atmospheric evasion (Fig. 1j,m); (iv) Snowmelt-induced soil water saturation, favouring the growth of moss and sedge-based ecosystems (e.g. Selvam et al., 2017; Tarnocai et al., 2009; Yu, 2011) and the retention of their organic matter (OM),.i.e., peat formation, not shown in Fig. 1 as this isn't represented in this model version, but is generated in a separate branch of ORCHIDEE (Qiu et al., 2018)).

Mid-summer river low-flow and a deeper active layer allow for the hydrological intrusion and leaching of older soil horizons (e.g. the top part of Pleistocene-era Yedoma soils), and their subsequent dissolved transport (e.g. Wickland et al., 2018). These sometimes-ancient low molecular weight carbon compounds appear to be preferentially and rapidly metabolised by microbes in headwater streams (Fig. 1j), which may constitute a significant fraction of aggregate summer CO_2 evasion in Arctic rivers (Denfeld et al., 2013; Vonk et al., 2015). This is likely due to the existence of a significant labile component of frozen carbon (Drake et al., 2015; Vonk et al., 2013; Woods et al., 2011);

CO_2 evasion rates from Arctic inland waters (Fig. 1j,e,m), which include both lakes and rivers, are estimated to be 40-84 TgC yr^{-1} (McGuire et al., 2009), of which 15-30 TgC yr^{-1} or one-third of the total inland evasion flux, is thought to come from rivers. Recent geo-statistically determined estimates of boreal lake annual emissions alone now stands at 74-347 TgC yr^{-1} (Hastie et al., 2018), although this is likely a substantial overestimate (Bogard et al., 2019), which potentially lowers the riverine fraction of total CO_2 evasion. These numbers should be compared with estimates of Pan-Arctic DOC discharge from rivers of 25-36 TgC yr^{-1}(Holmes et al., 2012; Raymond et al., 2007). The subsequent influx of terrestrial carbon to the shelf zone is thought to total 45-54 TgC yr^{-1}. Rivers supply the Arctic Ocean an estimated 34 Tg of carbon-equivalent DOC (DOC-C) yr^{-1} (Holmes et al., 2012), while depositing 5.8 Tg yr^{-1} of particulate carbon, these being sourced from those rivers draining low and high elevation headwaters, respectively (McClelland et al., 2016). These dynamics are all subject to considerable amplification by changes in temperature and hydrology (e.g. Drake et al., 2015; Frey and McClelland, 2009; Tank et al., 2018).

Average annual discharge in the Eurasian Arctic rivers has increased by at least 7% between 1936-1999 (Peterson et al., 2002), driven by increasing temperatures and runoff (Berezovskaya et al., 2005), and the subsequent interplay of increasing annual precipitation, decreasing snow depth and snow water equivalent (SWE) mass (Kunkel et al., 2016; Mudryk et al., 2015), and greater evapotranspiration (Suzuki et al., 2018; Zhang et al., 2009). Although net discharge trend rates over N. America were negative over the period 1964-2003, since 2003 they have been positive on average (Dery et al., 2016). These dynamic and largely increasing hydrologic flux trends point towards temperature and precipitation -driven changes in the soil column, in which increased soil water/snow thaw and microbial activity (Graham et al., 2012; MacKelprang et al., 2011; Schuur et al., 2009) converge to raise soil leaching and DOC export rates to the river basin and beyond (e.g. Vonk et al., (2015b)). Further, microbial activity generates its own heat, which incubation experiments have shown may be sufficient to significantly warm the soil further (Hollesen et al., 2015), in a positive feedback.

Arctic region fire events are also on the rise and likely to increase with temperature and severity over time (Ponomarev et al., 2016). The initial burning of biomass is accompanied by active layer deepening, priming of deeper soil horizons (De Baets et al., 2016), and a significant loading of pyrogenic DOC in Arctic watersheds, up to half of which is rapidly metabolised (Myers-Pigg et al., 2015).

In these contexts, the implications of (polar-amplified) warmer temperatures leading to active layer deepening towards the future (transition from Continuous to Discontinuous Permafrost, as shown in the upper/lower segments of Fig. 1) are clear and unique: potentially sizeable aquatic mobilisation and microbial metabolisation (Xue, 2017) of dissolved and eroded OM, deeper hydrological flow paths, an increase in total carbon and water mass and heat transfer to the aquatic network and, ultimately, the Arctic Ocean and atmosphere (Fig. 1i).

The advantage of having a terrestrial model that can be coupled to a marine component of an overarching global climate model (GCM) is in this case the representation of a consistent transboundary scheme, such that output from one model is integrated as input to another. This is particularly important given the context in which these terrestrial outflows occur :

Because of its small size, a uniquely large and shallow continental shelf, the global climatological significance of its seasonal sea ice (Rhein et al., 2013) and its rapid decline (Findlay et al., 2015), the Arctic Ocean has been described as a giant estuary (McClelland et al., 2012), acting as a funnel for the transport, processing and sedimentation of terrestrial OM. Because of its small surface area and shallow seas (Jakobsson, 2002), the Arctic Ocean holds relatively little volume and is consequently sensitive to inputs of freshwater, heat, alkalinity and nutrients that flush out from terrestrial sources, particularly at discharge peak.

High suspended particle loads in river water as they approach the mouth (Heim et al., 2014) cause lower light availability and water albedo and hence higher temperatures (Bauch et al., 2013; Janout et al., 2016), which can affect the near-shore sea ice extent, particularly in spring (Steele and Ermold, 2015). Volumes of riverine freshwater and total energy flux (Lammers et al., 2007) are expected to increase with warmer temperatures, along with an earlier discharge peak (Van Vliet et al., 2012, 2013). In doing so, freshwaters may in the future trigger earlier onset of ice retreat (Stroeve et al., 2014; Whitefield et al., 2015) via a freshwater albedo, ice melt, seawater albedo, ice melt, feedback, amplified by intermediary state variables such as water vapour and cloudiness (Serreze and Barry, 2011).

Both terrestrially-exported and older shelf carbon in the Arctic Ocean face considerable disruption (McGuire et al., 2009; Schuur et al., 2015) from the combined effects of increased freshwater, heat, sediment, nutrient and organic carbon flows from rapidly warming Arctic river watersheds, as well as those from melting sea ice, warmer marine water temperatures and geothermal heat sources (Janout et al., 2016; Shakhova et al., 2015). Because ORCHIDEE is a sub-component of the overarching IPSL ESM, there is scope for coupling riverine outputs of water, DOC, $CO_{2(aq)}$ and heat from the terrestrial model as input for the IPSL marine components (Fig. 1i). Nonetheless, these are not the objectives of the present paper, whose aim is rather to validate the simulated variable

output produced by the model described in detail below against observations and empirical knowledge for the Lena basin, but are included here descriptively to scope the plausible future applications of ORCHIDEE MICT-LEAK, given our present empirical understanding of their potential significance. The choice of the Lena River basin in Eastern Siberia as the watershed of study for model evaluation owes itself to its size, the presence of floodplains and mountain areas which allow us to test the model behavior for contrasting topography, the relatively low impact of damming on the river, given that ORCHIDEE only simulates undammed fluvial 'natural flow', and its mixture of continuous and discontinuous permafrost with tundra grassland in the north and boreal forests in the south, and is described in greater detail in Part 2 of this study.

The Methods section summarises the model structure and associated rationale for each of the model sub-branches or routines relevant to this study, and follows with the setup and rationale for the simulations carried out as validation exercises.

2 Methods

This section overviews the processes represented in the model being described in this manuscript, which is referred to as ORCHIDEE MICT-LEAK, hereafter referred to MICT-L for brevity. MICT-L is at its heart a merge of two distinct models : the high-latitude land surface component of the IPSL Earth System Model ORCHIDEE MICT, and the DOC-production and transport branch of ORCHIDEE's default or 'trunk' version (Krinner et al., 2005), ORCHILEAK. The original merger of these two code sets was between ORCHILEAK and ORCHIDEE-MICT, which are described in Camino-Serrano et al. (2018)/Lauerwald et al. (2017) and Guimberteau et al. (2018), respectively.

However, numerous improvements in code performance and process additions post-dating these publications have been included in this code. Furthermore, novel processes included in neither of these two core models are added to MICT-L, such as the diffusion of DOC through the soil column to represent its turbation and preferential stabilisation at depth in the soil, as described in Section.2.11.

In terms of code architecture, the resulting model is substantially different from either of its parents, owing to the fact that the two models were developed on the basis of ORCHIDEE trunk revisions 2728 and 3976 for ORCHILEAK and MICT respectively, which have a temporal model development distance of over 2 years, and subsequently evolved in their own directions. These foundational differences, which mostly affect the formulation of soil, carbon and hydrology schemes, mean that different aspects of each are necessarily forced into the subsequent code. Where these differences were considered scientific or code improvements, they were included in the resulting scheme. Despite architectural novelties introduced, MICT-L carries with it a marriage of much the same schemes detailed exhaustively in Guimberteau et al. (2018) and Lauerwald et al. (2017). As such, the following model description details only new elements of the model, those that are critical to the production and transport of DOC from permafrost regions, and parameterisations specific to this study (Fig. 2).

2.1 Model Description

MICT-L is based largely on ORCHIDEE-MICT, into which the DOC production, transport

and transformation processes developed in the ORCHILEAK model version and tested insofar only for the Amazon, have been transplanted, allowing for these same processes to be generated in high latitude regions with permafrost soils and a river flow regime dominated by snow melt. The description that ensues roughly follows the order of the carbon and water flow chain depicted in Fig. 2b. At the heart of the scheme is the vegetative production of carbon, which occurs along a spectrum of 13 plant functional types (PFTs) that differ from one another in terms of plant physiological and phenological uptake and release parameters (Krinner et al., 2005). Together, these determine grid-scale net primary production. In the northern high latitudes, the boreal trees (PFTs 7-9) and C3 grasses (PFT 10) dominate landscape biomass and primary production. Thus, in descending order yearly primary production over the Lena basin is roughly broken down between C3 grasses (48%), boreal needleleaf summergreen trees (27%), boreal needleleaf evergreen trees (12%), boreal broadleaf summergreen trees (8%) and temperate broad-leaved evergreen trees (6%). Naturally these basin aggregates are heterogeneously distributed along latitude and temperature contours, with grasses/tundra dominating at the high latitudes and (e.g.) temperate broadleaf trees existing only at the southern edges of the basin.

2.2 Biomass generation (Fig. 1a)

Biomass generation, consisting of foliage, roots, above and below –ground sap and heart wood, carbon reserves and fruit pools in the model, results in the transfer of these carbon stores to two downstream litter pools, the structural and metabolic litter (Figure 2b). This distinction, defined by lignin concentration of each biomass pool (Krinner et al., 2005), separates the relatively reactive litter fraction such as leafy matter from its less-reactive, recalcitrant counterpart (woody, 'structural' material), with the consequence that the turnover time of the latter is roughly four-fold that of the former. These two litter pools are further subdivided into above and below –ground pools, with the latter explicitly discretised over the first two metres of the soil column, a feature first introduced to the ORCHIDEE model by Camino-Serrano et al. (2014, 2018). This marks a significant departure from the original litter formulation in ORCHIDEE-MICT, in which the vertical distribution of litter influx to the soil carbon pool follows a prescribed root profile for each PFT. This change now allows for the production of DOC from litter explicitly at a given soil depth in permafrost soils.

2.3 DOC generation and leaching (Fig. 1b)

The vast majority of DOC produced by the model is generated initially from the litter pools via decomposition, such that half of all of the decomposed litter is returned to the atmosphere as CO_2, as defined by the microbial carbon use efficiency (CUE) –the fraction of carbon assimilated versus respired by microbes post-consumption –here set at 0.5 following Manzoni et al. (2012). The non-respired half of the litter feeds into 'Active', 'Slow' and 'Passive' free DOC pools, which correspond to DOC reactivity classes in the soil column in an analogous extension to the standard CENTURY formulation (Parton et al., 1987). Metabolic litter contributes exclusively to the Active DOC pool, while Structural litter feeds into the other two, the distribution between them dependent on the lignin content of the Structural litter. The reactive SOC pools then derive directly from this DOC reservoir, in that fractions of each DOC pool, defined again by the CUE, are directly transferred to three different SOC pools, while the remainder adds to the

heterotrophic soil respiration. Depending on clay content and bulk density of the soil, a fraction of DOC is adsorbed to the mineral soil and does not take part in these reactions until it is gradually desorbed when concentrations of free DOC decrease in the soil column. This scheme is explained in detail in Camino-Serrano (2018). The value of the fractional redistributions between free DOC and SOC after adsorption are shown in Fig. 2b.

The approximate ratio of relative residence times for the three SOC pools in our model (Active :Slow :Passive) is (1 :37:1618) at a soil temperature of 5°C, or 0.843 years, 31 yrs. and 1364 yrs. for the three pools respectively (Fig. 2b). These are based on our own exploratory model runs and subsequent calculations. The residence times of the active DOC pool is ~7 days (0.02 yrs.), while the slow and passive DOC pools both have a residence time of ~343 days (0.94 yrs.) at that same temperature. Upon microbial degradation in the model, SOC of each pool reverts either to DOC or to CO_2, the ratio between these determined again by the CUE which is set in this study at 0.5 for all donor pools, in keeping with the parameter configuration in Lauerwald et al., (2017) from Manzoni et al. (2012). This step in the chain of flows effectively represents leaching of SOC to DOC. Note that the reversion of SOC to DOC occurs only along Active-Active, Slow-Slow and Passive-Passive lines in Fig. 2b, while the conversion of DOC to SOC is distributed differently so as to build up a reasonable distribution of soil carbon stock reactivities. Note also that the microbial CUE is invoked twice in the chain of carbon breakdown, meaning that the 'effective' CUE of the SOC-litter system is approximately 0.25.

2.4 Throughfall and its DOC (Fig. 1c)

In MICT-L, DOC generation also occurs in the form of wet and dry atmospheric deposition and canopy exudation, collectively attributed to the throughfall, i.e. the amount of precipitation reaching the ground. Wet atmospheric deposition originates from organic compounds dispersed in atmospheric moisture which become deposited within rainfall, and are assumed here to maintain a constant concentration. This concentration we take from the average of reported rainfall DOC concentrations in the empirical literature measured at sites >55°N (Bergkvist and Folkeson, 1992; Clarke et al., 2007; Fröberg et al., 2006; Lindroos et al., 2011; Rosenqvist et al., 2010; Starr et al., 2003; Wu et al., 2010), whose value is 3 mgC L^{-1} of rainfall. Dry DOC deposition occurs through aerosol-bound organic compounds, here assumed to fall on the canopy ; canopy exudation refers to plant sugars exuded from the leaf surface (e.g. honey dew) or from their extraction by heterotrophs such as aphids. These two are lumped together in our estimates of canopy DOC generation (gDOC per g leaf carbon), which is calibrated as follows.

We take the average total observation-based throughfall DOC flux rate per m^2 of forest from the aforementioned literature bundle (15.7 gC m^{-2} yr^{-1}) and subtract from it the wet deposition component (product of rainfall over our simulation area and the rain DOC content). The remainder is then the canopy DOC, which we scale to the average leaf biomass simulated in a 107-year calibration run over the Lena river basin. From this we obtain a constant tree canopy DOC production rate of $9.2*10^{-4}$ g DOC-C per gram of leaf biomass per day (Eq. 1). This is the same for all PFTs except those representing crops, for which this value equals 0, reflecting how at a very general level, crops are small and

tend no to be characterised by high organic acid loss rates from leaves due to e.g. aphids, due to human control. Note that this production of DOC should be C initially fixed by photosynthesis, but it is here represented as an additional carbon flux. The dry deposition of DOC through the canopy is given by:

$$(1)\quad TF_{DRY} = M_{LEAF} * 9.2 * 10^{-4} \frac{dt}{day}$$

Where TF_{DRY} is dry deposition of DOC from the canopy, M_{LEAF} is leaf biomass, dt is the timestep of the surface hydrology and energy balance module (30min) and day is 24 hours. This accumulates in the canopy and can be flushed out with the throughfall and percolates into the soil surface or adds to the DOC stock of surface waters. The wet and canopy deposition which hits the soil is then assumed to be split evenly between the labile and refractory DOC pools (following Aitkenhead-Peterson et al., 2003).

2.5 Hydrological mobilisation of soil DOC (Fig. 1d)

All DOC pools, leached from the decomposition of either litter and SOC or being throughfall inputs, reside at this point in discrete layers within the soil column, but are now also available for vertical advection and diffusion, as well as lateral export from the soil column as a carbon tracer, via soil drainage and runoff.

Export of DOC from the soil to rivers occurs through surface runoff, soil-bottom drainage, or flooding events (see section 2.8, 'Representation of floodplain hydrology and their DOC budget'). Runoff is activated when the maximum water infiltration rate of the specific soil has been exceeded, meaning that water arrives at the soil surface faster than it can enter, forcing it to be transported laterally across the surface. DOC is drawn up into this runoff water flux from the first 5 layers of the soil column, which correspond to a cumulative source depth of 4.5cm.

Drainage of DOC occurs first as its advection between the discrete soil layers, and its subsequent export from the 11th layer, which represents the bottom of the first 2m of the soil column, from which export is calculated as a proportion of the DOC concentration at this layer. Below this, soil moisture and DOC concentrations are no longer explicitly calculated, except in the case that they are cryoturbated below this, up to a depth of 3m. DOC drainage is proportional to but not a constant multiplier of the water drainage rate for two reasons. First, as it water percolates through the soil column, it carries DOC along from one layer to another through the entirety of the soil column, but this percolation is blocked when the soil is entirely frozen, i.e. it is assumed that all soil pores are filled with ice which blocks percolation. This implies that DOC transport is not just determined by what enters from the top but also by the below ground production from litter, the sorption and de-sorption to and from particulate soil organic carbon in the soil column, DOC mineralisation within the soil column, and water vertical transport entraining DOC between the non-frozen soil layers using the hydraulic conductivity calculated by the model as a function of soil texture, soil carbon and time-dependent soil moisture (Guimberteau et al., 2018).

Simon Bowring 3/7/y 08:50
Supprimé: ,

Simon Bowring 3/7/y 08:52
Supprimé: its decomposition

Secondly, in order to account for preferential flow paths in the soil created by the subsoil actions of flora and fauna, and for the existence of non-homogenous soil textures at depth that act as aquitards, DOC infiltration must account for the fact that area-aggregated soils drain more slowly, increasing the residence time of DOC in the soil. Thus a reduction factor which reduces the vertical advection of DOC in soil solution by 80% compared to the advection is applied to represent a slow down in DOC percolation through the soil and increase its residence time there.

In MICT-L, as in ORCHILEAK, a 'poor soils' module reads off from a map giving fractional coverage of land underlain by Podzols and Arenosols at the 0.5° grid-scale, as derived from the Harmonized World Soil Database (Nachtergaele, 2010). Due to their low pH and nutrient levels, areas identified by this soil-type criterion experience soil organic matter decomposition rates half that of other soils (Lauerwald et al. (2017), derived from Bardy et al. (2011); Vitousek & Sanford (1986); Vitousek & Hobbie (2000)). To account for the very low DOC-filtering capacity of these coarse-grained, base- and clay-poor soils (DeLuca & Boisvenue (2012), Fig. 2b), no reduction factor in DOC advection rate relative to that of water in the soil column is applied when DOC is generated within these "poor soils".

By regulating both decomposition and soil moisture flux, the "poor soil" criterion effectively serves a similar if not equal function to a soil 'tile' for DOC infiltration in the soil column (inset box of Fig. 1), because soil tiles (forest, grassland/tundra/cropland and bare soil) are determinants of soil hydrology which affects moisture-limited decomposition. Here however, the 'poor soil' criteria is applied uniformly across the three soil tiles of each grid cell. This modulation in MICT-L is of significance for the Arctic region, given that large fractions of the discontinuous permafrost region are underlain by Podzols, particularly in Eurasia. For the Arctic as a whole, Podzols cover ~15% of total surface area (DeLuca and Boisvenue, 2012). Further, in modelled frozen soils, a sharp decline in hydraulic conductivity is imposed by the physical barrier of ice filling the soil pores, which retards the flow of water to depth in the soil, imposing a cap on drainage and thus potentially increasing runoff of water laterally, across the soil surface (Gouttevin et al., 2012). In doing so, frozen soil layers overlain by liquid soil moisture will experience enhanced residence times of water in the carbon-rich upper soil layers, potentially enriching their DOC load. Note that ice wedges, an important component of permafrost landscapes and their thaw processes, are not included in the current terrestrial representation, but have been previously simulated in other models (Lee et al., 2014).

Thus, for all the soil layers in the first 2m, DOC stocks are controlled by production from litter and SOC decay, their advection, diffusion, and consumption by DOC mineralisation, as well as buffering by adsorption and desorption processes.

2.6 Routing Scheme:

The routing scheme in ORCHIDEE, first described in detail in Ngo-Duc et al. (2007) and presented after some version iterations in Guimberteau et al. (2012), is the module which when activated, represents the transport of water collected by the runoff and drainage simulated by the model along the prescribed river network in a given watershed. In doing so, its purpose is to coarsely represent the hydrologic coupling

between precipitation inputs to the model and subsequent terrestrial runoff and drainage (or evaporation) calculated by it on the one hand, and the eventual discharge of freshwater to the marine domain, on the other. In other words, the routing scheme simulates the transport of water by rivers and streams, by connecting rainfall and continental river discharge with the land surface.

To do so, the routing scheme first inputs a map of global watersheds at the 0.5 degree scale (Oki et al., 1999; Vorosmarty et al., 2000) which gives watershed and sub-basin boundaries and the direction of water-flow based on topography to the model. The water flows themselves are comprised of three distinct linear reservoirs within each sub-basin ('slow', 'fast', 'stream'). Each water reservoir is represented at the scale (here: 4 sub-grid units per grid cell), and updated with the lateral in- and outflows at a daily time-step. The 'slow' water reservoir aggregates the soil drainage, i.e. the vertical outflow from the 11^{th} layer (2 m depth) of the soil column, effectively representing 'shallow groundwater' transport and storage. The 'fast' water reservoir aggregates surface runoff simulated in the model, effectively representing overland hydrologic flow. The 'fast' water reservoir aggregates surface runoff simulated in the model, effectively representing overland hydrologic flow. The 'slow' and 'fast' water reservoirs feed a delayed outflow to the 'stream' reservoir' of the next downstream sub-grid quadrant

The water residence time in each reservoir depends on the nature of the reservoir (increasing residence time in the order: stream < fast < slow reservoir). More generally, residence time locally decreases with topographic slope and the grid-cell length, used as a proxy for the main tributary length (Ducharne et al., 2003; Guimberteau et al., 2012). This is done to reproduce the hydrological effects of geomorphological and topographic factors in Manning's equation (Manning, 1891) and determines the time that water and DOC remain in soils prior to entering the river network or groundwater. In this way the runoff and drainage are exported from sub-unit to sub-unit and from grid-cell to grid-cell.

2.7 Grid-scale water and carbon routing (Fig. 1f, 1g)

Water-borne, terrestrially-derived DOC and dissolved CO_2 in the soil solution are exported over the land surface using the same routing scheme. When exported from soil or litter, DOC remains differentiated in the numerical simulations according to its initial reactivity within the soil (Active, Slow, Passive). However, because the terrestrial Slow and Passive DOC pools (Camino-Serrano et al., 2018) are given the same residence time, these two pools are merged when exported (Lauerwald et al., 2017): Active DOC flows into a Labile DOC hydrological export pool, while the Slow and Passive DOC pools flow into a Refractory DOC hydrological pool (Fig. 2b), owing to the fact that the residence time of these latter soil DOC pools is the same in their original (ORCHIDEE-SOM) formulation (Camino-Serrano et al., 2018), and retained and merged into a single hydrological DOC pool in Lauerwald et al. (2017). The water residence times in each reservoir of each sub-grid scale quadrant determine the decomposition of DOC into CO_2 within water reservoirs, before non-decomposed DOC is passed on to the next reservoir in the downstream sub-grid quadrant.

The river routing calculations, which occur at a daily timestep, are then aggregated to one-day for the lateral transfer of water, $CO_{2(aq)}$ and DOC from upstream grid to downstream grid according to the river network. Note that carbonate chemistry in rivers and total alkalinity routing are not calculated here.

In this framework, the 'fast' and 'slow' residence times of the water pools in the routing scheme determine the time that water and DOC remains in overland and groundwater flow before entering the river network. Note that while we do not explicitly simulate headwaters as they exist in a geographically determinant way in the real world, we do simulate what happens to the water before it flows into a water body large enough to be represented in the routing scheme by the water pool called 'stream', representing a real-world river of stream order 4 or higher. The 'fast' reservoir is thus the runoff water flow that is destined for entering the 'stream' water reservoir, and implicitly represents headwater streams of Strahler order 1 to 3 by filling the spatial and temporal niche between overland runoff and the river stem. The dynamics of headwater hydrological and DOC dynamics (Section 2.10) are of potentially great significance with respect to carbon processing, as headwater catchments have been shown to be 'hotspots' of carbon metabolisation and outgassing in Arctic rivers, despite their relatively small areal fraction (Denfeld et al., 2013; Drake et al., 2015; Mann et al., 2015; Suzuki et al., 2006; Venkiteswaran et al., 2014; Vonk et al., 2013, 2015a, 2015b). Thus, in what follows in this study, we refer to what in the code are called the 'fast' and 'stream' pools, which represent the small streams and large stream or river pools, respectively, using 'stream' and 'river' to denote these from hereon in.

Furthermore, the differentiated representation of water pools as well as mean grid cell slope, combined with the dynamic active layer simulated for continuous versus discontinuous permafrost, is important for reproducing the phenomena observed by Kutscher et al. (2017) and Zhang et al. (2017) for sloping land as shown on the right hand side of Fig. 1. In discontinuous permafrost and permafrost free regions, these phenomena encompass landscape processes (sub-grid in the model), through which water flow is able to re-infiltrate the soil column and so leach more refractory DOC deeper in the soil column, leading to a more refractory signal in the drainage waters. In contrast, in continuous permafrost region, the shallow active layer will inhibit the downward re-infiltration flux of water and encourage leaching at the more organic-rich and labile surface soil layer, resulting in a more labile DOC signal from the drainage in these areas (Fig. 1). In addition, places with higher elevation and slope in these regions tend to experience extreme cold, leading to lower NPP and so DOC leaching. The re-infiltration processes mentioned are thought to be accentuated in areas with higher topographic relief (Jasechko et al., 2016), which is why they are represented on sloping areas in Fig. 1.

2.8 Representation of floodplain hydrology and their DOC budget (Fig. 1e,1h)

The third terrestrial DOC export pathway in MICT-L is through flooding of floodplains, a transient period that occurs when stream water is forced by high discharge rates over the river 'banks' and flows onto a flat floodplain area of the grid cell that the river crosses, thus inundating the soil. Such a floodplain area is represented as a fraction of a grid-cell with the maximum extent of inundation, termed the 'potential flooded area' being predefined from a forcing file (Tootchi et al., 2019). Here, the DOC pools that are

already being produced in these inundated areas from litter and SOC decomposition in the first 5 layers of the soil column are directly absorbed by the overlying flood waters. These flood waters may then either process the DOC directly, via oxidisation to CO_2, (Sections 2.10, 2.11) or return them to the river network, as floodwaters recede to the river main stem, at which point they join the runoff and drainage export flows from upstream.

MICT-L includes the floodplain hydrology part of the routing scheme (D'Orgeval et al., 2008; Guimberteau et al., 2012), as well as additions and improvements described in Lauerwald et al. (2017). The spatial areas that are available for potential flooding are pre-defined by an input map originally based on the map of Prigent et al. (2007). However, for this study, we used an alternative map of the "regularly flooded areas" derived from the method described in Tootchi et al., (2019), which in this study uses an improved input potential flooding area forcing file specific to the Lena basin, that combines three high-resolution surface water and inundation datasets derived from satellite imagery: GIEMS-D15 (Fluet-Chouinard et al., 2015), which results from the downscaling of the map of Prigent et al. (2007) at 15-arc-sec (ca 500 m at Equator); ESA-CCI land cover (at 300 m ~ 10 arc-sec); and JRC surface water at 1 arc-sec (Pekel et al., 2016). The 'fusion' approach followed by this forcing dataset stems from the assumption that the potential flooding areas identified by the different datasets are all valid despite their uncertainties, although none of them is exhaustive. The resulting map was constructed globally at the 15 arc-sec resolution and care was taken to exclude large permanent lakes from the potential flooding area based on the HydroLAKES database (Messager et al., 2016). In the Lena river basin, the basin against which we evaluate ORCHIDEE MICT-LEAK in Part 2 of this study, this new potential floodplains file gives a maximum floodable area of 12.1% ($2.4*10^5$ km^2) of the $2.5*10^6$ km^2 basin, substantially higher than previous estimates of 4.2% by Prigent et al. (2007).

With this improved forcing, river discharge becomes available to flood a specific pre-defined floodplain grid fraction, creating a temporary floodplains hydrologic reservoir, whose magnitude is defined by the excess of discharge at that point over a threshold value, given by the median simulated water storage of water in each grid cell over a 30 year period. The maximum extent of within-grid flooding is given by another threshold, the calculated height of flood waters beyond which it is assumed that the entire grid is inundated. This height, which used to be fixed at 2 m, is now determined by the 90th percentile of all flood water height levels calculated per grid cell from total water storage of that grid cell over a reference simulation period for the Lena basin, using the same methodology introduced by Lauerwald et al. (2017). The residence time of water on the floodplains (τ_{flood}) is a determinant of its resulting DOC concentration, since during this period it appropriates all DOC produced by the top 5 layers of the soil column.

2.9 Oceanic outflow (Fig. 1i)

Routing of water and DOC through the river network ultimately lead to their export from the terrestrial system at the river mouth (Fig. 1), which for high latitude rivers are almost entirely sub-deltas of the greater 'estuary', described by McClelland et al. (2012), draining into the Arctic Ocean. Otherwise, the only other loss pathway for carbon export once in the river network is through its decomposition to CO_2 and subsequent

escape to the atmosphere from the river surface. DOC decomposition is ascribed a constant fraction for the labile and refractory DOC pools of 0.3 d^{-1} and 0.01 d^{-1} at 25°C, respectively, these modulated by a water-temperature dependent Arrhenius rate term. Because the concentration of dissolved CO_2 (referred to as $CO_{2(aq.)}$) in river water is derived not only from in-stream decomposition of DOC, but also from $CO_{2(aq.)}$ inputs from the decomposition of litter, SOC and DOC both in upland soils and in inundated soils, the model also represents the lateral transport of $CO_{2(aq.)}$ from soils through the river network. Note that autochtonous primary production and derivative carbon transformations are ignored here, as they are considered relatively minor contributors in the Arctic lateral flux system (Cauwet and Sidorov, 1996; Sorokin and Sorokin, 1996).

2.10 Dissolved CO_2 export and river evasion (Fig. 1j)

Soil $CO_{2(aq.)}$ exports are simulated by first assuming a constant concentration of $CO_{2(aq.)}$ with surface runoff and drainage water fluxes, of 20 and 2 mgC L^{-1}, corresponding to a *p*CO2 of 50000 μ atm and 5000 μ atm at 25°C in the soil column, respectively. These quantities are then scaled with total (root, microbial, litter) soil respiration by a scaling factor first employed in Lauerwald et al. (2019, *in review*). In the high latitudes soil respiration is dominantly controlled by microbial decomposition, and for the Lena basin initial model tests suggest that its proportional contribution to total respiration is roughly 90%, versus 10% from root respiration. Thus $CO_{2(aq.)}$ enters and circulates the rivers via the same routing scheme as that for DOC and river water. The lateral transfers of carbon are aggregated from the 30 minute time steps at which they are calculated, with a 48 timestep period, so that they occur within the model as a daily flux. The calculation of the river network pCO_2 can then be made from $CO_{2(aq.)}$ and its equilibrium with the atmosphere, which is a function of its solubility (K_{CO2}) with respect to the temperature of the water surface T_{WATER} (Eq.2).

$$(2)\quad pCO_{2_{POOL}} = \frac{[CO_{2(aq)}]}{12.011 * K_{CO_2}}$$

Where the pCO_2 (atm.) of a given (e.g. 'stream', 'fast', 'slow' and floodplain) water pool (pCO_{2POOL}) is given by the dissolved CO_2 concentration in that pool [$CO_{2(aq)}$], the molar weight of carbon (12.011 g mol^{-1}) and K_{CO2}. Water temperature (T_{WATER}, (°C)) isn't simulated by the model, but is derived here from the average daily surface temperature (T_{GROUND}, (°C)) in the model (Eq. 3), a derivation calculated for ORCHIDEE by Lauerwald et al. (2017) and retained here. Note that while dissolved CO_2 enters from the terrestrial reservoir from organic matter decomposition, it is also generated *in situ* within the river network as DOC is respired microbially.

With our water temperature estimate, both K_{CO2} and the Schmidt number (*Sc,* Eq. 4) from Wanninkhof (1992) can be calculated, allowing for simulation of actual gas exchange velocities from standard conditions. The Schmidt number links the gas transfer velocity of any soluble gas (in this case carbon dioxide) from the water surface to water temperature. For more on the Schmidt number see (Wanninkhof, 2014, 1992). The CO_2 that evades is then subtracted from the [$CO_{2(aq)}$] stocks of each of the different hydrologic reservoirs –river, flood and stream.

$$(3)\quad T_{WATER} = 6.13^{\circ}C + (0.8 * T_{GROUND})$$

$$(4)\ Sc = \left((1911 - 118.11) * T_{WATER}\right) + \left(3.453 * T_{WATER}^2\right) - \left(0.0413 * T_{WATER}^3\right)$$

CO_2 evasion is therefore assumed to originate from the interplay of CO_2 solubility, relative gradient in partial pressures of CO_2 between air and water, and gas exchange kinetics. Evasion as a flux from river and floodplain water surfaces is calculated at a daily timestep, however in order to satisfy the sensitivity of the relative gradient of partial pressures of CO_2 in the water column and atmosphere to both CO_2 inputs and evasion, the pCO_2 of water is calculated at a more refined 6 minute timestep. The daily lateral flux of CO_2 inputs to the water column are thus equally broken up into 240 (6 min.) segments per day and distributed to the pCO_2 calculation. Other relevant carbon processing pathways, such as the photochemical breakdown of riverine dissolved organic carbon, are not explicitly included here, despite the suggestion by some studies that the photochemical pathway dominate DOC processing in Arctic streams (e.g. Cory et al., 2014). Rather, these processes are bundled into the aggregate decomposition rates used in the model, which thus include both microbial and photochemical oxidation. This is largely because it is unclear how different factors contribute to breaking down DOC in a dynamic environment and also the extent to which our DOC decomposition and CO_2 calculations implicitly include both pathways –e.g. to what extent the equations and concepts used in their calculation confound bacterial with photochemical causation, since both microbial activity and incident UV light are a function of temperature and total incident light.

2.11 Soil layer processes: turbation (Fig. 1k), **adsorption** (Fig. 1l)

The soil carbon module is discretised into a 32-layer scheme totalling 38m depth, which it shares with the soil thermodynamics to calculate temperature through the entire column. An aboveground snow module (Wang et al., 2013) is discretised into 3 layers of differing thickness, heat conductance and density, which collectively act as a thermodynamically-insulating intermediary between soil and atmosphere (Fig. 2a). Inputs to the three soil carbon pools are resolved only for the top 2m of the soil, where litter and DOC are exchanged with SOC in decomposition and adsorption/desorption processes. Decomposition of SOC pools, calculated in each soil layer, is dependent on soil temperature, moisture and texture (Koven et al., 2009; Zhu et al., 2016), while vertical transfer of SOC is enabled by representation of cryoturbation (downward movement of matter due to repeated freeze-thaw) in permafrost regions, and bioturbation (by soil organisms) in non-permafrost regions in terms of a diffusive flux.

Cryoturbation, given a diffusive mixing rate (Diff) of 0.001 $m^2\ yr^{-1}$ (Koven et al., 2009), is possible to 3 m depth (diffusive rate declines linearly to zero from active layer bottom to 3 m), and extends the soil column carbon concentration depth in permafrost regions from 2 m. Bioturbation is possible to 2 m depth, with a mixing rate of 0.0001 $m^2\ yr^{-1}$ (Koven et al., 2013) declining to zero at 2 m (Eq. 5). In MICT-L, these vertical exchanges in the soil column are improved on. Now, we explicitly include the cryoturbation and bioturbation of both belowground litter and DOC. These were not possible in ORCHIDEE-MICT because, for the former, the belowground litter distribution was not explicitly discretised or vertically dynamic, and for the latter because DOC was not produced in prior versions. Diffusion is given by :

$$((5)\ )\quad \frac{\delta DOC_i(z)}{\delta t} = IN_{DOC_i}(z) - k_i(z) * \phi * DOC_i(z) + Diff\frac{\delta DOC_i^2(z)}{\delta z^2}$$

Where DOC_i is the DOC in pool i at depth z, (gC m^{-3}) IN_{DOCi} the inflow of carbon to that pool ($gCm^{-3}d^{-1}$), k_i the decomposition rate of that pool (d^{-1}), Φ the temperature dependent rate modifier for DOC decomposition and *Diff* the diffusion coefficient ($m^2\,yr^{-1}$). The vertical diffusion of DOC in non-permafrost soils represented here (that is, the non-cryoturbated component) appears to be consistent with recent studies reporting an increased retention of DOC in the deepening active layer of organic soils (Zhang et al., 2017). This vertical translocation of organic carbon, whether in solid/liquid phase appears to be an important component of the high rates of SOC buildup observed at depth in deep permafrost soils.

2.11 Priming (Fig. 1m)

MICT-L also incorporates a scheme for the 'priming' of organic matter decomposition, a process in which the relative stability of SOC is impacted by the intrusion of or contact with SOC of greater reactivity, resulting in enhanced rates of decomposition. This was first introduced by Guenet et al. (2016) and updated in Guenet et al. (2018). This process has shown itself to be of potentially large significance for SOC stocks and their respiration in high latitude regions, in empirical in situ and soil incubation studies (De Baets et al., 2016; Walz et al., 2017; Wild et al., 2014, 2016; Zhang et al., 2017), as well as modelling exercises (Guenet et al., 2018). Here, priming of a given soil pool is represented through the decomposition of soil carbon (*dSOC/dt*) by the following equation :

$$(6)\quad \frac{dSOC}{dt} = IN_{SOC} - k * (1 - e^{-c*FOC}) * SOC * \Theta * \phi * \gamma$$

Where IN_{SOC} is the carbon input to that pool, k is the SOC decomposition rate ($1/dt$), *FOC* (Kg) is a stock of matter interacting with this SOC pool to produce priming, c is a parameter controlling this interaction, *SOC* is the SOC reservoir (Kg), and θ, Φ and γ the zero-dimensional moisture, temperature and soil texture rate modifiers that modulate decomposition in the code, and are originally determined by the CENTURY formulation (Parton et al., 1987) and subsequently re-estimated to include priming in Guenet et al., (2016, 2018)."

.. The variable *FOC* ('fresh organic carbon') is an umbrella term used for specifying all of the carbon pools which together constitute that carbon which is considered potential priming donor material –ie. more labile – to a given receptor carbon pool. Thus, for the slow soil carbon pool FOC incorporates the active soil carbon pool plus the above and below ground structural and metabolic litter pools, because these pools are donors to the slow pool, and considered to accelerate its turnover through priming. Importantly, previous studies with priming in ORCHIDEE employed this scheme on a version which resolves neither the vertical discretisation of the soil column nor the explicit vertical diffusion processes presented here. This is potentially significant, since the vertical diffusion of relatively reactive matter may strongly impact (accelerate) the decomposition of low reactivity matter in the deeper non-frozen horizons of high latitude soils, while the explicit discretisation of the soil column is a significant improvement in terms of the accuracy of process-representation within the column

itself.

Other carbon-relevant schemes included in MICT-L are: A prognostic fire routine (SPITFIRE), calibrated for the trunk version of ORCHIDEE (Yue et al., 2016) is available in our code but not activated in the simulations conducted here. As a result, we do not simulate the ~13% of Arctic riverine DOC attributed to biomass burning by Myers-Pigg et al. (2015), or the ~8% of DOC discharge to the Arctic Ocean from the same source (Stubbins et al., 2017). Likewise, a crop harvest module consistent with that in ORCHIDEE-MICT exists in MICT-L but remains deactivated for our simulations.

A module introduced in the last version of ORCHIDEE-MICT (Guimberteau et al., 2018), in which the soil thermal transfer and porosity and moisture are strongly affected by SOC concentration, is deactivated here, because it is inconsistent with the new DOC scheme. Specifically, while carbon is conserved in both MICT and MICT-L soil schemes, MICT-L introduces a new reservoir into which part of the total organic carbon in the soil –the DOC –must now go. This then lowers the SOC concentration being read by this thermix module, causing significant model artefact in soil thermodynamics and hydrology in early exploratory simulations. Ensuring compatibility of this routine with the DOC scheme will be a focal point of future developments in MICT-L. Other processes being developed for ORCHIDEE-MICT, including a high latitude peat formation (Qiu et al., 2018), methane production and microbial heat generating processes that are being optimised and calibrated, are further pending additions to this particular branch of the ORCHIDEE-MICT series.

3 Soil Carbon Spinup and Simulation Protocol

The soil carbon spinup component of ORCHIDEE, which is available to both its trunk and MICT branches, was omitted from this first version of MICT-L, owing to the code burden required for ensuring compatibility with the soil carbon scheme in MICT-L. However, because we are simulating high latitude permafrost regions, having a realistic soil carbon pool at the outset of the simulations is necessary if we are to untangle the dynamics of SOC and DOC with a changing environment. Because the soil carbon spinup in ORCHIDEE-MICT is normally run over more than 10,000 years (Guimberteau et al., 2108), and because running MICT-L for this simulation period in its normal, non-spinup simulation mode would impose an unreasonable burden on computing resources, here we directly force the soil carbon output from a MICT spinup directly into the restart file of a MICT-L simulation.

A 20,000 year spinup loop over 1961-1990 (these years chosen to mimic coarsely warmer mid-Holocene climate) -forced by GSWP-3 climatology, whose configuration derives directly from that used in Guimberteau et al. (2018), was thus used to replace the three soil carbon pool values from a 1-year MICT-L simulation to set their initial values. A conversion of this soil carbon from volumetric to areal units was applied, owing to different read/write standards in ORCHILEAK versus ORCHIDEE-MICT. This artificially imposed, MICT-derived SOC stock would then have to be exposed to MICT-L code, whose large differences in soil carbon module architecture as compared to MICT, would drive a search for new equilibrium soil carbon stocks.

Due to the long residence times of the passive SOC pool, reaching full equilibrium for it

requires a simulation length on the order of 20,000y –again an overburden. As we are interested primarily in DOC in this study, which derives mostly from the Active and Slow SOC pools, the model was run until these two pools reached a quasi-steady state equilibria (Part 2 Supplement, Fig. S1). This was done by looping over the same 30 year cycle (1901-1930) of climate forcing data from GSWP-3 during the pre-industrial period (Table 1) and the first year (1901) of a prescribed vegetation map (ESA CCI Land Cover Map, Bontemps et al., (2013)) –to ensure equilibrium of DOC, dissolved CO_2 and Active and Slow SOC pools is driven not just by a single set of environmental factors in one year –for a total of 400 years. The parameter configuration adhered as close as possible to that used in the original ORCHIDEE-MICT spinup simulations, to avoid excessive equilibrium drift from the original SOC state (Fig. 3).

4 Conclusion

This first part of a two-part study has described a new branch of the high latitude version of ORCHIDEE-MICT land surface model, in which the production, transport and transformation of DOC and dissolved CO_2 in soils and along the inland water network of explicitly-represented northern permafrost regions has been implemented for the first time. Novel processes with respect to ORCHIDEE-MICT include the discretisation of litter inputs to the soil column, the production of DOC and $CO_{2(aq.)}$ from organic matter and decomposition, respectively, transport of DOC into the river routing network and its potential mineralisation to $CO_{2(aq.)}$ in the water column, as well as subsequent evasion from the water surface to the atmosphere. In addition, an improved floodplains representation has been implemented which allows for the hydrologic cycling of DOC and CO_2 in these inundated areas. In addition to descriptions of these processes, this paper outlines the protocols and configuration adopted for simulations using this new model that will be used for its evaluation over the Lena river basin in the second part of this study.

Code and data availability

The source code for ORCHIDEE MICT-LEAK revision 5459 is available via http://forge.ipsl.jussieu.fr/orchidee/wiki/GroupActivities/CodeAvalaibilityPublication/ORCHIDEE_gmd-2018-MICT-LEAK_r5459

Primary data and scripts used in the analysis and other supplementary information that may be useful in reproducing the author's work can be obtained by contacting the corresponding author.

Authors' contribution

SB coded this model version, conducted the simulations and wrote the main body of the paper. RL gave consistent input to the coding process and made numerous code improvements and bug fixes. BG advised on the inclusion of priming processes in the model and advised on the study design and model configuration; DZ gave input on the modelled soil carbon processes and model configuration. MG, AT and AD contributed to

improvements in hydrological representation and floodplain forcing data. PC oversaw all developments leading to the publication of this study. All authors contributed to suggestions regarding the final content of the study.

Competing interests

The authors declare no competing financial interests.

Acknowledgements

Simon Bowring acknowledges funding from the European Union's Horizon 2020 research and innovation program under the Marie Sklodowska-Curie grant agreement No. 643052, 'C-CASCADES' program. Simon Bowring received a PhD grant. Matthieu Guimberteau acknowledges funding from the European Research Council Synergy grant ERC-2013-SyG-610028 IMBALANCE-P. Ronny Lauerwald acknowledges funding from the European Union's Horizon 2020 research and innovation program under grant agreement no.703813 for the Marie Sklodowska-Curie European Individual Fellowship "C-Leak".

References:

Aitkenhead-Peterson, J. A., McDowell, W. H. and Neff, J. C.: Sources, Production, and Regulation of Allochthonous Dissolved Organic Matter Inputs to Surface Waters, in Aquatic Ecosystems., 2003.

De Baets, S., Van de Weg, M. J., Lewis, R., Steinberg, N., Meersmans, J., Quine, T. A., Shaver, G. R. and Hartley, I. P.: Investigating the controls on soil organic matter decomposition in tussock tundra soil and permafrost after fire, Soil Biol. Biochem., doi:10.1016/j.soilbio.2016.04.020, 2016.

Bardy, M., Derenne, S., Allard, T., Benedetti, M. F. and Fritsch, E.: Podzolisation and exportation of organic matter in black waters of the Rio Negro (upper Amazon basin, Brazil), Biogeochemistry, doi:10.1007/s10533-010-9564-9, 2011.

Bauch, D., Hölemann, J. A., Nikulina, A., Wegner, C., Janout, M. A., Timokhov, L. A. and Kassens, H.: Correlation of river water and local sea-ice melting on the Laptev Sea shelf (Siberian Arctic), J. Geophys. Res. Ocean., doi:10.1002/jgrc.20076, 2013.

Berezovskaya, S., Yang, D. and Hinzman, L.: Long-term annual water balance analysis of the Lena River, Glob. Planet. Change, doi:10.1016/j.gloplacha.2004.12.006, 2005.

Bergkvist, B. O. and Folkeson, L.: Soil acidification and element fluxes of a Fagus sylvatica forest as influenced by simulated nitrogen deposition, Water, Air, Soil Pollut., doi:10.1007/BF00482753, 1992.

Bogard, M. J., Kuhn, C. D., Johnston, S. E., Striegl, R. G., Holtgrieve, G. W., Dornblaser, M. M., Spencer, R. G. M., Wickland, K. P. and Butman, D. E.: Negligible cycling of terrestrial carbon in many lakes of the arid circumpolar landscape, Nat. Geosci., doi:10.1038/s41561-019-0299-5, 2019.

Bontemps, S., Defourny, P., Radoux, J., Van Bogaert, E., Lamarche, C., Achard, F., Mayaux, P., Boettcher, M., Brockmann, C., Kirches, G., Zülkhe, M., Kalogirou, V., Seifert, F. . and Arino, O.: Consistent global land cover maps for climate modelling communities: current achievements of the ESA' and cover CCI, in ESA Living Planet Symposium 2013., 2013.

Camino-Serrano, M., Gielen, B., Luyssaert, S., Ciais, P., Vicca, S., Guenet, B., Vos, B. De, Cools, N., Ahrens, B., Altaf Arain, M., Borken, W., Clarke, N., Clarkson, B., Cummins, T., Don, A., Pannatier, E. G., Laudon, H., Moore, T., Nieminen, T. M., Nilsson, M. B., Peichl, M., Schwendenmann, L., Siemens, J. and Janssens, I.: Linking variability in soil solution

926 dissolved organic carbon to climate, soil type, and vegetation type, Global Biogeochem.
927 Cycles, doi:10.1002/2013GB004726, 2014.
928 Camino-Serrano, M., Guenet, B., Luyssaert, S., Ciais, P., Bastrikov, V., De Vos, B., Gielen, B.,
929 Gleixner, G., Jornet-Puig, A., Kaiser, K., Kothawala, D., Lauerwald, R., Peñuelas, J.,
930 Schrumpf, M., Vicca, S., Vuichard, N., Walmsley, D. and Janssens, I. A.: ORCHIDEE-SOM:
931 Modeling soil organic carbon (SOC) and dissolved organic carbon (DOC) dynamics along
932 vertical soil profiles in Europe, Geosci. Model Dev., doi:10.5194/gmd-11-937-2018,
933 2018.
934 Cauwet, G. and Sidorov, I.: The biogeochemistry of Lena River: Organic carbon and
935 nutrients distribution, in Marine Chemistry., 1996.
936 Clarke, N., Wu, Y. and Strand, L. T.: Dissolved organic carbon concentrations in four
937 Norway spruce stands of different ages, Plant Soil, doi:10.1007/s11104-007-9384-4,
938 2007.
939 Cory, R. M., Ward, C. P., Crump, B. C. and Kling, G. W.: Sunlight controls water column
940 processing of carbon in arctic fresh waters, Science (80-.)., doi:10.1126/science.1253119, 2014.
941 doi:10.1126/science.1253119, 2014.
942 D'Orgeval, T., Polcher, J. and De Rosnay, P.: Sensitivity of the West African hydrological
943 cycle in ORCHIDEE to infiltration processes, Hydrol. Earth Syst. Sci., doi:10.5194/hess-
944 12-1387-2008, 2008.
945 DeLuca, T. H. and Boisvenue, C.: Boreal forest soil carbon: Distribution, function and
946 modelling, Forestry, doi:10.1093/forestry/cps003, 2012.
947 Denfeld, B., Frey, K. and Sobczak, W.: Summer CO 2 evasion from streams and rivers in
948 the Kolyma River basin, north-east Siberia, Polar …, doi:10.3402/polar.v32i0.19704,
949 2013.
950 Dery, S. J., Stadnyk, T. A., MacDonald, M. K. and Gauli-Sharma, B.: Recent trends and
951 variability in river discharge across northern Canada, Hydrol. Earth Syst. Sci.,
952 doi:10.5194/hess-20-4801-2016, 2016.
953 Drake, T. W., Wickland, K. P., Spencer, R. G. M., McKnight, D. M. and Striegl, R. G.: Ancient
954 low–molecular-weight organic acids in permafrost fuel rapid carbon dioxide production
955 upon thaw, Proc. Natl. Acad. Sci., doi:10.1073/pnas.1511705112, 2015.
956 Ducharne, A., Golaz, C., Leblois, E., Laval, K., Polcher, J., Ledoux, E. and De Marsily, G.:
957 Development of a high resolution runoff routing model, calibration and application to
958 assess runoff from the LMD GCM, J. Hydrol., doi:10.1016/S0022-1694(03)00230-0,
959 2003.
960 Findlay, H. S., Gibson, G., Kędra, M., Morata, N., Orchowska, M., Pavlov, A. K., Reigstad, M.,
961 Silyakova, A., Tremblay, J.-É., Walczowski, W., Weydmann, A. and Logvinova, C.:
962 Responses in Arctic marine carbon cycle processes: conceptual scenarios and
963 implications for ecosystem function, Polar Res., doi:10.3402/polar.v34.24252, 2015.
964 Fluet-Chouinard, E., Lehner, B., Rebelo, L. M., Papa, F. and Hamilton, S. K.: Development
965 of a global inundation map at high spatial resolution from topographic downscaling of
966 coarse-scale remote sensing data, Remote Sens. Environ., doi:10.1016/j.rse.2014.10.015,
967 2015.
968 Frey, K. E. and McClelland, J. W.: Impacts of permafrost degradation on arctic river
969 biogeochemistry, Hydrol. Process., doi:10.1002/hyp.7196, 2009.
970 Fröberg, M., Berggren, D., Bergkvist, B., Bryant, C. and Mulder, J.: Concentration and
971 fluxes of dissolved organic carbon (DOC) in three Norway spruce stands along a climatic
972 gradient in Sweden, Biogeochemistry, doi:10.1007/s10533-004-0564-5, 2006.
973 Gouttevin, I., Menegoz, M., Dominé, F., Krinner, G., Koven, C., Ciais, P., Tarnocai, C. and
974 Boike, J.: How the insulating properties of snow affect soil carbon distribution in the

975 continental pan-Arctic area, J. Geophys. Res. Biogeosciences,
976 doi:10.1029/2011JG001916, 2012.
977 Graham, D. E., Wallenstein, M. D., Vishnivetskaya, T. A., Waldrop, M. P., Phelps, T. J.,
978 Pfiffner, S. M., Onstott, T. C., Whyte, L. G., Rivkina, E. M., Gilichinsky, D. A., Elias, D. A.,
979 MacKelprang, R., Verberkmoes, N. C., Hettich, R. L., Wagner, D., Wullschleger, S. D. and
980 Jansson, J. K.: Microbes in thawing permafrost: The unknown variable in the climate
981 change equation, ISME J., doi:10.1038/ismej.2011.163, 2012.
982 Guenet, B., Moyano, F. E., Peylin, P., Ciais, P. and Janssens, I. A.: Towards a representation
983 of priming on soil carbon decomposition in the global land biosphere model ORCHIDEE
984 (version 1.9.5.2), Geosci. Model Dev., doi:10.5194/gmd-9-841-2016, 2016.
985 Guenet, B., Camino-Serrano, M., Ciais, P., Tifafi, M., Maignan, F., Soong, J. L. and Janssens,
986 I. A.: Impact of priming on global soil carbon stocks, Glob. Chang. Biol.,
987 doi:10.1111/gcb.14069, 2018.
988 Guimberteau, M., Drapeau, G., Ronchail, J., Sultan, B., Polcher, J., Martinez, J. M., Prigent,
989 C., Guyot, J. L., Cochonneau, G., Espinoza, J. C., Filizola, N., Fraizy, P., Lavado, W., De
990 Oliveira, E., Pombosa, R., Noriega, L. and Vauchel, P.: Discharge simulation in the sub-
991 basins of the Amazon using ORCHIDEE forced by new datasets, Hydrol. Earth Syst. Sci.,
992 doi:10.5194/hess-16-911-2012, 2012.
993 Guimberteau, M., Zhu, D., Maignan, F., Huang, Y., Yue, C., Dantec-N d lec, S., Ottl, C., Jornet-
994 Puig, A., Bastos, A., Laurent, P., Goll, D., Bowring, S., Chang, J., Guenet, B., Tifafi, M., Peng,
995 S., Krinner, G., Ducharne, A. s., Wang, F., Wang, T., Wang, X., Wang, Y., Yin, Z., Lauerwald,
996 R., Joetzjer, E., Qiu, C., Kim, H. and Ciais, P.: ORCHIDEE-MICT (v8.4.1), a land surface
997 model for the high latitudes: model description and validation, Geosci. Model Dev.,
998 doi:10.5194/gmd-11-121-2018, 2018.
999 Hastie, A., Lauerwald, R., Weyhenmeyer, G., Sobek, S., Verpoorter, C. and Regnier, P.: CO2
1000 evasion from boreal lakes: Revised estimate, drivers of spatial variability, and future
1001 projections, Glob. Chang. Biol., doi:10.1111/gcb.13902, 2018.
1002 Heim, B., Abramova, E., Doerffer, R., Günther, F., Hölemann, J., Kraberg, A., Lantuit, H.,
1003 Loginova, A., Martynov, F., Overduin, P. P. and Wegner, C.: Ocean colour remote sensing
1004 in the southern laptev sea: Evaluation and applications, Biogeosciences, doi:10.5194/bg-
1005 11-4191-2014, 2014.
1006 Hollesen, J., Matthiesen, H., Møller, A. B. and Elberling, B.: Permafrost thawing in organic
1007 Arctic soils accelerated by ground heat production, Nat. Clim. Chang.,
1008 doi:10.1038/nclimate2590, 2015.
1009 Holmes, R. M., McClelland, J. W., Peterson, B. J., Tank, S. E., Bulygina, E., Eglinton, T. I.,
1010 Gordeev, V. V., Gurtovaya, T. Y., Raymond, P. A., Repeta, D. J., Staples, R., Striegl, R. G.,
1011 Zhulidov, A. V. and Zimov, S. A.: Seasonal and Annual Fluxes of Nutrients and Organic
1012 Matter from Large Rivers to the Arctic Ocean and Surrounding Seas, Estuaries and
1013 Coasts, doi:10.1007/s12237-011-9386-6, 2012.
1014 Hugelius, G., Bockheim, J. G., Camill, P., Elberling, B., Grosse, G., Harden, J. W., Johnson, K.,
1015 Jorgenson, T., Koven, C. D., Kuhry, P., Michaelson, G., Mishra, U., Palmtag, J., Ping, C.-L.,
1016 O'Donnell, J., Schirrmeister, L., Schuur, E. A. G., Sheng, Y., Smith, L. C., Strauss, J. and Yu, Z.:
1017 A new data set for estimating organic carbon storage to 3m depth in soils of the
1018 northern circumpolar permafrost region, EARTH Syst. Sci. DATA, doi:10.5194/essd-5-
1019 393-2013, 2013.
1020 Hugelius, G., Strauss, J., Zubrzycki, S., Harden, J. W., Schuur, E. A. G., Ping, C. L.,
1021 Schirrmeister, L., Grosse, G., Michaelson, G. J., Koven, C. D., O'Donnell, J. A., Elberling, B.,
1022 Mishra, U., Camill, P., Yu, Z., Palmtag, J. and Kuhry, P.: Estimated stocks of circumpolar
1023 permafrost carbon with quantified uncertainty ranges and identified data gaps,

1024 Biogeosciences, doi:10.5194/bg-11-6573-2014, 2014.
1025 Jakobsson, M.: Hypsometry and volume of the Arctic Ocean and its constituent seas,
1026 Geochemistry, Geophys. Geosystems, doi:10.1029/2001GC000302, 2002.
1027 Janout, M., HÃ¶lemann, J., Juhls, B., Krumpen, T., Rabe, B., Bauch, D., Wegner, C., Kassens,
1028 H. and Timokhov, L.: Episodic warming of near-bottom waters under the Arctic sea ice
1029 on the central Laptev Sea shelf, Geophys. Res. Lett., doi:10.1002/2015GL066565, 2016.
1030 Jasechko, S., Kirchner, J. W., Welker, J. M. and McDonnell, J. J.: Substantial proportion of
1031 global streamflow less than three months old, Nat. Geosci., doi:10.1038/ngeo2636, 2016.
1032 Kicklighter, D. W., Hayes, D. J., Mcclelland, J. W., Peterson, B. J., Mcguire, A. D. and Melillo,
1033 J. M.: Insights and issues with simulating terrestrial DOC loading of Arctic river
1034 networks, Ecol. Appl., doi:10.1890/11-1050.1, 2013.
1035 Koven, C., Friedlingstein, P., Ciais, P., Khvorostyanov, D., Krinner, G. and Tarnocai, C.: On
1036 the formation of high-latitude soil carbon stocks: Effects of cryoturbation and insulation
1037 by organic matter in a land surface model, Geophys. Res. Lett.,
1038 doi:10.1029/2009GL040150, 2009.
1039 Koven, C. D., Riley, W. J., Subin, Z. M., Tang, J. Y., Torn, M. S., Collins, W. D., Bonan, G. B.,
1040 Lawrence, D. M. and Swenson, S. C.: The effect of vertically resolved soil biogeochemistry
1041 and alternate soil C and N models on C dynamics of CLM4, Biogeosciences,
1042 doi:10.5194/bg-10-7109-2013, 2013.
1043 Koven, C. D., Schuur, E. A. G., Schädel, C., Bohn, T. J., Burke, E. J., Chen, G., Chen, X., Ciais, P.,
1044 Grosse, G., Harden, J. W., Hayes, D. J., Hugelius, G., Jafarov, E. E., Krinner, G., Kuhry, P.,
1045 Lawrence, D. M., MacDougall, A. H., Marchenko, S. S., McGuire, A. D., Natali, S. M.,
1046 Nicolsky, D. J., Olefeldt, D., Peng, S., Romanovsky, V. E., Schaefer, K. M., Strauss, J., Treat, C.
1047 C. and Turetsky, M.: A simplified, data-constrained approach to estimate the permafrost
1048 carbon-climate feedback, Philos. Trans. R. Soc. A Math. Phys. Eng. Sci.,
1049 doi:10.1098/rsta.2014.0423, 2015.
1050 Krinner, G., Viovy, N., de Noblet-Ducoudré, N., Ogée, J., Polcher, J., Friedlingstein, P., Ciais,
1051 P., Sitch, S. and Prentice, I. C.: A dynamic global vegetation model for studies of the
1052 coupled atmosphere-biosphere system, Global Biogeochem. Cycles,
1053 doi:10.1029/2003GB002199, 2005.
1054 Kunkel, K. E., Robinson, D. A., Champion, S., Yin, X., Estilow, T. and Frankson, R. M.:
1055 Trends and Extremes in Northern Hemisphere Snow Characteristics, Curr. Clim. Chang.
1056 Reports, doi:10.1007/s40641-016-0036-8, 2016.
1057 Kutscher, L., Mörth, C. M., Porcelli, D., Hirst, C., Maximov, T. C., Petrov, R. E. and
1058 Andersson, P. S.: Spatial variation in concentration and sources of organic carbon in the
1059 Lena River, Siberia, J. Geophys. Res. Biogeosciences, doi:10.1002/2017JG003858, 2017.
1060 Lammers, R. B., Pundsack, J. W. and Shiklomanov, A. I.: Variability in river temperature,
1061 discharge, and energy flux from the Russian pan-Arctic landmass, J. Geophys. Res.
1062 Biogeosciences, doi:10.1029/2006JG000370, 2007.
1063 Lauerwald, R., Regnier, P., Camino-Serrano, M., Guenet, B., Guimberteau, M., Ducharne,
1064 A., Polcher, J. and Ciais, P.: ORCHILEAK (revision 3875): A new model branch to simulate
1065 carbon transfers along the terrestrial-aquatic continuum of the Amazon basin, Geosci.
1066 Model Dev., doi:10.5194/gmd-10-3821-2017, 2017.
1067 Lee, H., Swenson, S. C., Slater, A. G. and Lawrence, D. M.: Effects of excess ground ice on
1068 projections of permafrost in a warming climate, Environ. Res. Lett., doi:10.1088/1748-
1069 9326/9/12/124006, 2014.
1070 Lindroos, A. J., Derome, J., Derome, K. and Smolander, A.: The effect of scots pine, norway
1071 spruce and silver birch on the chemical composition of stand throughfall and upper soil
1072 percolation water in northern Finland, Boreal Environ. Res., 2011.

MacKelprang, R., Waldrop, M. P., Deangelis, K. M., David, M. M., Chavarria, K. L., Blazewicz, S. J., Rubin, E. M. and Jansson, J. K.: Metagenomic analysis of a permafrost microbial community reveals a rapid response to thaw, Nature, doi:10.1038/nature10576, 2011.
Mann, P. J., Eglinton, T. I., McIntyre, C. P., Zimov, N., Davydova, A., Vonk, J. E., Holmes, R. M. and Spencer, R. G. M.: Utilization of ancient permafrost carbon in headwaters of Arctic fluvial networks, Nat. Commun., doi:10.1038/ncomms8856, 2015.
Manning, R.: On the Flow of Water in Open Channels and Pipes, Trans. Inst. Civ. Eng. Irel., doi:10.1021/bi2010619, 1891.
Manzoni, S., Taylor, P., Richter, A., Porporato, A. and Ågren, G. I.: Environmental and stoichiometric controls on microbial carbon-use efficiency in soils, New Phytol., doi:10.1111/j.1469-8137.2012.04225.x, 2012.
McClelland, J. W., Holmes, R. M., Dunton, K. H. and Macdonald, R. W.: The Arctic Ocean Estuary, Estuaries and Coasts, doi:10.1007/s12237-010-9357-3, 2012.
McClelland, J. W., Holmes, R. M., Peterson, B. J., Raymond, P. A., Striegl, R. G., Zhulidov, A. V., Zimov, S. A., Zimov, N., Tank, S. E., Spencer, R. G. M., Staples, R., Gurtovaya, T. Y. and Griffin, C. G.: Particulate organic carbon and nitrogen export from major Arctic rivers, Global Biogeochem. Cycles, doi:10.1002/2015GB005351, 2016.
McGuire, A. D., Anderson, L. G., Christensen, T. R., Dallimore, S., Guo, L., Hayes, D. J., Heimann, M., Lorenson, T. D., Macdonald, R. W. and Roulet, N.: Sensitivity of the carbon cycle in the Arctic to climate change, Ecol. Monogr., doi:10.1890/08-2025.1, 2009.
Messager, M. L., Lehner, B., Grill, G., Nedeva, I. and Schmitt, O.: Estimating the volume and age of water stored in global lakes using a geo-statistical approach, Nat. Commun., doi:10.1038/ncomms13603, 2016.
Mudryk, L. R., Derksen, C., Kushner, P. J. and Brown, R.: Characterization of Northern Hemisphere snow water equivalent datasets, 1981-2010, J. Clim., doi:10.1175/JCLI-D-15-0229.1, 2015.
Myers-Pigg, A. N., Louchouarn, P., Amon, R. M. W., Prokushkin, A., Pierce, K. and Rubtsov, A.: Labile pyrogenic dissolved organic carbon in major Siberian Arctic rivers: Implications for wildfire-stream metabolic linkages, Geophys. Res. Lett., doi:10.1002/2014GL062762, 2015.
Nachtergaele, F. et al.: The harmonized world soil database, FAO, ISRIC,ISSCAS, JRC, doi:3123, 2010.
Ngo-Duc, T., Laval, K., Ramillien, G., Polcher, J. and Cazenave, A.: Validation of the land water storage simulated by Organising Carbon and Hydrology in Dynamic Ecosystems (ORCHIDEE) with Gravity Recovery and Climate Experiment (GRACE) data, Water Resour. Res., doi:10.1029/2006WR004941, 2007.
O'Donnell, J. A., Aiken, G. R., Swanson, D. K., Panda, S., Butler, K. D. and Baltensperger, A. P.: Dissolved organic matter composition of Arctic rivers: Linking permafrost and parent material to riverine carbon, Global Biogeochem. Cycles, doi:10.1002/2016GB005482, 2016.
Oki, T., Nishimura, T. and Dirmeyer, P. A.: Assessment of annual runoff from land surface models using Total Runoff Integrating Pathways (TRIP), J. Meteorol. Soc. Japan, 1999.
Parton, W. J., Schimel, D. S., Cole, C. V. and Ojima, D. S.: Analysis of Factors Controlling Soil Organic Matter Levels in Great Plains Grasslands, Soil Sci. Soc. Am. J., 1987.
Pekel, J.-F., Cottam, A., Gorelick, N. and Belward, A. S.: Global Surface Water - Data Users Guide (JRC) High-resolution mapping of global surface water and its long-term changes, Nature, doi:10.1038/nature20584, 2016.
Peterson, B. J., Holmes, R. M., McClelland, J. W., Vörösmarty, C. J., Lammers, R. B.,

Shiklomanov, A. I., Shiklomanov, I. A. and Rahmstorf, S.: Increasing river discharge to the Arctic Ocean, Science (80-.)., doi:10.1126/science.1077445, 2002.
Ponomarev, E. I., Kharuk, V. I. and Ranson, K. J.: Wildfires dynamics in Siberian larch forests, Forests, doi:10.3390/f7060125, 2016.
Prigent, C., Papa, F., Aires, F., Rossow, W. B. and Matthews, E.: Global inundation dynamics inferred from multiple satellite observations, 1993-2000, J. Geophys. Res. Atmos., doi:10.1029/2006JD007847, 2007.
Qiu, C., Zhu, D., Ciais, P., Guenet, B., Krinner, G., Peng, S., Aurela, M., Bernhofer, C., Brümmer, C., Bret-Harte, S., Chu, H., Chen, J., Desai, A. R., Dušek, J., Euskirchen, E. S., Fortuniak, K., Flanagan, L. B., Friborg, T., Grygoruk, M., Gogo, S., Grünwald, T., Hansen, B. U., Holl, D., Humphreys, E., Hurkuck, M., Kiely, G., Klatt, J., Kutzbach, L., Largeron, C., Laggoun-Défarge, F., Lund, M., Lafleur, P. M., Li, X., Mammarella, I., Merbold, L., Nilsson, M. B., Olejnik, J., Ottosson-Löfvenius, M., Oechel, W., Parmentier, F. J. W., Peichl, M., Pirk, N., Peltola, O., Pawlak, W., Rasse, D., Rinne, J., Shaver, G., Peter Schmid, H., Sottocornola, M., Steinbrecher, R., Sachs, T., Urbaniak, M., Zona, D. and Ziemblinska, K.: ORCHIDEE-PEAT (revision 4596), a model for northern peatland CO2, water, and energy fluxes on daily to annual scales, Geosci. Model Dev., doi:10.5194/gmd-11-497-2018, 2018.
Raymond, P. A., McClelland, J. W., Holmes, R. M., Zhulidov, A. V., Mull, K., Peterson, B. J., Striegl, R. G., Aiken, G. R. and Gurtovaya, T. Y.: Flux and age of dissolved organic carbon exported to the Arctic Ocean: A carbon isotopic study of the five largest arctic rivers, Global Biogeochem. Cycles, doi:10.1029/2007GB002934, 2007.
Rhein, M., Rintoul, S., Aoki, S., Campos, E., Chambers, D., Feely, R. A., Gulev, S., Johnson, G., Josey, S., Kostianoy, A., Mauritzen, C., Roemmich, D., Talley, L., Wang, F. and IPCC: Observations: Ocean. In: Climate Change 2013: The Physical Science Basis. Contribution of Working Group I to the Fifth Assessment Report of the Intergovernmental Panel on Climate Change., 2013.
Rosenqvist, L., Hansen, K., Vesterdal, L. and van der Salm, C.: Water balance in afforestation chronosequences of common oak and Norway spruce on former arable land in Denmark and southern Sweden, Agric. For. Meteorol., doi:10.1016/j.agrformet.2009.10.004, 2010.
Schuur, E. A. G., Vogel, J. G., Crummer, K. G., Lee, H., Sickman, J. O. and Osterkamp, T. E.: The effect of permafrost thaw on old carbon release and net carbon exchange from tundra, Nature, doi:10.1038/nature08031, 2009.
Schuur, E. A. G., McGuire, A. D., Schädel, C., Grosse, G., Harden, J. W., Hayes, D. J., Hugelius, G., Koven, C. D., Kuhry, P., Lawrence, D. M., Natali, S. M., Olefeldt, D., Romanovsky, V. E., Schaefer, K., Turetsky, M. R., Treat, C. C. and Vonk, J. E.: Climate change and the permafrost carbon feedback, Nature, doi:10.1038/nature14338, 2015.
Selvam, B. P., Lapierre, J. F., Guillemette, F., Voigt, C., Lamprecht, R. E., Biasi, C., Christensen, T. R., Martikainen, P. J. and Berggren, M.: Degradation potentials of dissolved organic carbon (DOC) from thawed permafrost peat, Sci. Rep., doi:10.1038/srep45811, 2017.
Serreze, M. C. and Barry, R. G.: Processes and impacts of Arctic amplification: A research synthesis, Glob. Planet. Change, doi:10.1016/j.gloplacha.2011.03.004, 2011.
Shakhova, N., Semiletov, I., Sergienko, V., Lobkovsky, L., Yusupov, V., Salyuk, A., Salomatin, A., Chernykh, D., Kosmach, D., Panteleev, G., Nicolsky, D., Samarkin, V., Joye, S., Charkin, A., Dudarev, O., Meluzov, A. and Gustafsson, O.: The East Siberian Arctic Shelf: Towards further assessment of permafrost-related methane fluxes and role of sea ice, Philos. Trans. R. Soc. A Math. Phys. Eng. Sci., doi:10.1098/rsta.2014.0451, 2015.
Smith, L. C. and Pavelsky, T. M.: Estimation of river discharge, propagation speed, and

hydraulic geometry from space: Lena River, Siberia, Water Resour. Res., doi:10.1029/2007WR006133, 2008.
Sorokin, Y. I. and Sorokin, P. Y.: Plankton and primary production in the Lena River Estuary and in the south-eastern Laptev sea, Estuar. Coast. Shelf Sci., doi:10.1006/ecss.1996.0078, 1996.
Spencer, R. G. M., Mann, P. J., Dittmar, T., Eglinton, T. I., McIntyre, C., Holmes, R. M., Zimov, N. and Stubbins, A.: Detecting the signature of permafrost thaw in Arctic rivers, Geophys. Res. Lett., doi:10.1002/2015GL063498, 2015.
Starr, M., Lindroos, A. J., Ukonmaanaho, L., Tarvainen, T. and Tanskanen, H.: Weathering release of heavy metals from soil in comparison to deposition, litterfall and leaching fluxes in a remote, boreal coniferous forest, Appl. Geochemistry, doi:10.1016/S0883-2927(02)00157-9, 2003.
Steele, M. and Ermold, W.: Loitering of the retreating sea ice edge in the Arctic Seas, J. Geophys. Res. Ocean., doi:10.1002/2015JC011182, 2015.
Stroeve, J. C., Markus, T., Boisvert, L., Miller, J. and Barrett, A.: Changes in Arctic melt season and implications for sea ice loss, Geophys. Res. Lett., doi:10.1002/2013GL058951, 2014.
Stubbins, A., Mann, P. J., Powers, L., Bittar, T. B., Dittmar, T., McIntyre, C. P., Eglinton, T. I., Zimov, N. and Spencer, R. G. M.: Low photolability of yedoma permafrost dissolved organic carbon, J. Geophys. Res. Biogeosciences, doi:10.1002/2016JG003688, 2017.
Suzuki, K., Konohira, E., Yamazaki, Y., Kubota, J., Ohata, T. and Vuglinsky, V.: Transport of organic carbon from the Mogot Experimental Watershed in the southern mountainous taiga of eastern Siberia, Hydrol. Res., doi:10.2166/nh.2006.015, 2006.
Suzuki, K., Matsuo, K., Yamazaki, D., Ichii, K., Iijima, Y., Papa, F., Yanagi, Y. and Hiyama, T.: Hydrological variability and changes in the Arctic circumpolar tundra and the three largest pan-Arctic river basins from 2002 to 2016, Remote Sens., doi:10.3390/rs10030402, 2018.
Tank, S. E., Fellman, J. B., Hood, E. and Kritzberg, E. S.: Beyond respiration: Controls on lateral carbon fluxes across the terrestrial-aquatic interface, Limnol. Oceanogr. Lett., doi:10.1002/lol2.10065, 2018.
Tarnocai, C., Canadell, J. G., Schuur, E. A. G., Kuhry, P., Mazhitova, G. and Zimov, S.: Soil organic carbon pools in the northern circumpolar permafrost retion, Global Biogeochem. Cycles, doi:Gb2023\n10.1029/2008gb003327, 2009.
Tootchi, A., Jost, A. and Ducharne, A.: Multi-source global wetland maps combining surface water imagery and groundwater constraints, Earth Syst. Sci. Data, doi:10.5194/essd-11-189-2019, 2019.
Venkiteswaran, J. J., Schiff, S. L. and Wallin, M. B.: Large carbon dioxide fluxes from headwater boreal and sub-boreal streams, PLoS One, doi:10.1371/journal.pone.0101756, 2014.
Vitousek, P. M. and Hobbie, S.: Heterotrophic nitrogen fixation in decomposing litter: Patterns and regulation, Ecology, doi:10.1890/0012-9658(2000)081[2366:HNFIDL]2.0.CO;2, 2000.
Vitousek, P. M. and Sanford, R. L.: Nutrient Cycling in Moist Tropical Forest, Ecology, doi:0.1146/annurev.es.17.110186.001033, 1986.
Van Vliet, M. T. H., Yearsley, J. R., Franssen, W. H. P., Ludwig, F., Haddeland, I., Lettenmaier, D. P. and Kabat, P.: Coupled daily streamflow and water temperature modelling in large river basins, Hydrol. Earth Syst. Sci., doi:10.5194/hess-16-4303-2012, 2012.
Van Vliet, M. T. H., Franssen, W. H. P., Yearsley, J. R., Ludwig, F., Haddeland, I.,

Lettenmaier, D. P. and Kabat, P.: Global river discharge and water temperature under climate change, Glob. Environ. Chang., doi:10.1016/j.gloenvcha.2012.11.002, 2013.
Vonk, J. E., Mann, P. J., Davydov, S., Davydova, A., Spencer, R. G. M., Schade, J., Sobczak, W. V., Zimov, N., Zimov, S., Bulygina, E., Eglinton, T. I. and Holmes, R. M.: High biolability of ancient permafrost carbon upon thaw, Geophys. Res. Lett., doi:10.1002/grl.50348, 2013.
Vonk, J. E., Tank, S. E., Mann, P. J., Spencer, R. G. M., Treat, C. C., Striegl, R. G., Abbott, B. W. and Wickland, K. P.: Biodegradability of dissolved organic carbon in permafrost soils and aquatic systems: A meta-analysis, Biogeosciences, doi:10.5194/bg-12-6915-2015, 2015a.
Vonk, J. E., Tank, S. E., Bowden, W. B., Laurion, I., Vincent, W. F., Alekseychik, P., Amyot, M., Billet, M. F., Canário, J., Cory, R. M., Deshpande, B. N., Helbig, M., Jammet, M., Karlsson, J., Larouche, J., MacMillan, G., Rautio, M., Walter Anthony, K. M. and Wickland, K. P.: Reviews and Syntheses: Effects of permafrost thaw on arctic aquatic ecosystems, Biogeosciences Discuss., doi:10.5194/bgd-12-10719-2015, 2015b.
Vorosmarty, C. J., Fekete, B. M., Meybeck, M. and Lammers, R. B.: Global system of rivers: Its role in organizing continental land mass and defining land-To-Ocean linkages, Global Biogeochem. Cycles, doi:10.1029/1999GB900092, 2000.
Walz, J., Knoblauch, C., Böhme, L. and Pfeiffer, E. M.: Regulation of soil organic matter decomposition in permafrost-affected Siberian tundra soils - Impact of oxygen availability, freezing and thawing, temperature, and labile organic matter, Soil Biol. Biochem., doi:10.1016/j.soilbio.2017.03.001, 2017.
Wang, T., Ottlé, C., Boone, A., Ciais, P., Brun, E., Morin, S., Krinner, G., Piao, S. and Peng, S.: Evaluation of an improved intermediate complexity snow scheme in the ORCHIDEE land surface model, J. Geophys. Res. Atmos., doi:10.1002/jgrd.50395, 2013.
Wanninkhof, R.: Relationship between wind speed and gas exchange over the ocean revisited, Limnol. Oceanogr. Methods, doi:10.4319/lom.2014.12.351, 2014.
Wanninkhof, R. H.: Relationship between wind speed and gas exchange, J. Geophys. Res., doi:10.1029/92JC00188, 1992.
Whitefield, J., Winsor, P., McClelland, J. and Menemenlis, D.: A new river discharge and river temperature climatology data set for the pan-Arctic region, Ocean Model., doi:10.1016/j.ocemod.2014.12.012, 2015.
Wickland, K. P., Waldrop, M. P., Aiken, G. R., Koch, J. C., Jorgenson, M. T. and Striegl, R. G.: Dissolved organic carbon and nitrogen release from boreal Holocene permafrost and seasonally frozen soils of Alaska, Environ. Res. Lett., doi:10.1088/1748-9326/aac4ad, 2018.
Wild, B., Schnecker, J., Alves, R. J. E., Barsukov, P., Bárta, J., Čapek, P., Gentsch, N., Gittel, A., Guggenberger, G., Lashchinskiy, N., Mikutta, R., Rusalimova, O., Šantrůčková, H., Shibistova, O., Urich, T., Watzka, M., Zrazhevskaya, G. and Richter, A.: Input of easily available organic C and N stimulates microbial decomposition of soil organic matter in arctic permafrost soil, Soil Biol. Biochem., doi:10.1016/j.soilbio.2014.04.014, 2014.
Wild, B., Gentsch, N., Capek, P., Diáková, K., Alves, R. J. E., Bárta, J., Gittel, A., Hugelius, G., Knoltsch, A., Kuhry, P., Lashchinskiy, N., Mikutta, R., Palmtag, J., Schleper, C., Schnecker, J., Shibistova, O., Takriti, M., Torsvik, V. L., Urich, T., Watzka, M., Šantrūcková, H., Guggenberger, G. and Richter, A.: Plant-derived compounds stimulate the decomposition of organic matter in arctic permafrost soils, Sci. Rep., doi:10.1038/srep25607, 2016.
Woods, G. C., Simpson, M. J., Pautler, B. G., Lamoureux, S. F., Lafrenière, M. J. and Simpson, A. J.: Evidence for the enhanced lability of dissolved organic matter following permafrost slope disturbance in the Canadian High Arctic, Geochim. Cosmochim. Acta, doi:10.1016/j.gca.2011.08.013, 2011.

Wu, Y., Clarke, N. and Mulder, J.: Dissolved organic carbon concentrations in throughfall and soil waters at level II monitoring plots in norway: Short- and long-term variations, Water. Air. Soil Pollut., doi:10.1007/s11270-009-0073-1, 2010.
Xue, K.: Tundra soil carbon is vulnerable to rapid microbial decomposition under climatewarming, Nat. Clim. Chang., doi:10.1038/NCLIMATE2940, 2017.
Ye, B., Yang, D., Zhang, Z. and Kane, D. L.: Variation of hydrological regime with permafrost coverage over Lena Basin in Siberia, J. Geophys. Res. Atmos., doi:10.1029/2008JD010537, 2009.
Yu, Z.: Holocene carbon flux histories of the world's peatlands: Global carbon-cycle implications, Holocene, doi:10.1177/0959683610386982, 2011.
Yue, C., Ciais, P., Zhu, D., Wang, T., Peng, S. S. and Piao, S. L.: How have past fire disturbances contributed to the current carbon balance of boreal ecosystems?, Biogeosciences, doi:10.5194/bg-13-675-2016, 2016.
Zhang, K., Kimball, J. S., Mu, Q., Jones, L. A., Goetz, S. J. and Running, S. W.: Satellite based analysis of northern ET trends and associated changes in the regional water balance from 1983 to 2005, J. Hydrol., doi:10.1016/j.jhydrol.2009.09.047, 2009.
Zhang, X., Hutchings, J. A., Bianchi, T. S., Liu, Y., Arellano, A. R. and Schuur, E. A. G.: Importance of lateral flux and its percolation depth on organic carbon export in Arctic tundra soil: Implications from a soil leaching experiment, J. Geophys. Res. Biogeosciences, doi:10.1002/2016JG003754, 2017.
Zhu, D., Peng, S., Ciais, P., Zech, R., Krinner, G., Zimov, S. and Grosse, G.: Simulating soil organic carbon in yedoma deposits during the Last Glacial Maximum in a land surface model, Geophys. Res. Lett., doi:10.1002/2016GL068874, 2016.
Zubrzycki, S., Kutzbach, L., Grosse, G. and Desyatkin, A.: Organic carbon and total nitrogen stocks in soils of the Lena River Delta, Biogeosciences, doi:10.5194/bg-10-3507-2013, 2013.

Tables and Figures:

Table 1: Data type, name and sources of data files used to drive the model in the study simulations.

Data Type	Name	Source
Vegetation Map	ESA CCI Land Cover Map	Bontemps et al., 2013
Topographic Index	STN-30p	Vörösmarty et al., 2000
Stream flow direction	STN-30p	Vörösmarty et al., 2000
River surface area		Lauerwald et al., 2015
Soil texture class		Reynolds et al. 1999
Climatology	GSWP3 v0, 1 degree	http://hydro.iis.u-tokyo.ac.jp/GSWP3/
Potential floodplains	Multi-source global wetland maps	Tootchi et al., 2019
Poor soils	Harmonized World Soil Database map	Nachtergaele et al., 2010
Spinup Soil Carbon Stock	20ky ORCHIDEE-MICT soil carbon spinup	Based on config. in Guimberteau et al. (2018)

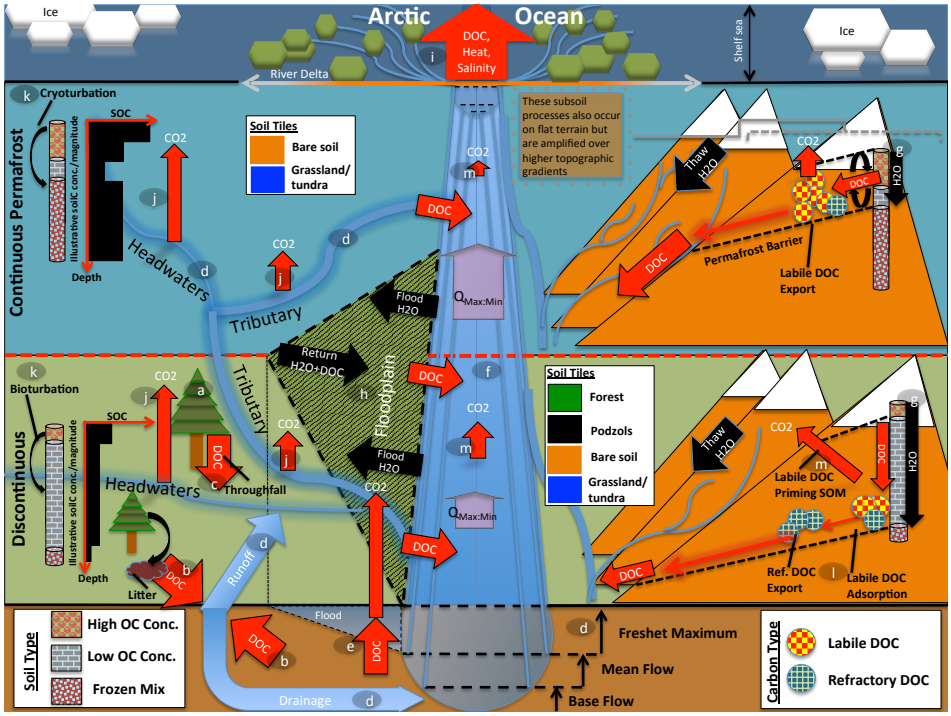

Figure 1: Cartoon diagram illustrating the landscape-scale emergent phenomena observed in high-latitude river systems that are captured by the processes represented in this model. Here, the terrestrial area is shown, in vertically-ascending order, as subsoil, discontinuous permafrost, continuous permafrost and the maritime boundary. Note that 'tributaries' in the Figure may be represented in the model by either the 'fast' or 'stream' pool, depending on their size. Representative soil types, their distributions and carbon concentrations are shown for the two permafrost zones, as well as the different dynamics occuring on 'flat' (left) and 'sloping' land (right) arising from their permafrost designation. Carbon exports from one subsystem to another are shown in red. The relative strength of the same processes ocurring in each permafrost band are indicated by relative arrow size. Note that the high CO_2 evasion in headwaters versus tributaries versus mainstem is shown here. Proposed and modelled mechanisms of soil carbon priming, adsorption and rapid metabolisation are shown. The arrows $Q_{Max:Min}$ refer to the ratio of maximum to minimum discharge at a given point in the river, the ratio indicating hydrologic volatility, whose magnitude is influenced by permafrost coverage. Soil tiles, a model construct used for modulating soil permeability and implicit/explicit decomposition, are shown to indicate the potential differences in these dynamics for the relevant permafrost zones. Note that the marine shelf sea system, as shown in the uppermost rectangle, is not simulated in this model, although our outputs can be coupled for that purpose. Letter markings mark processes of carbon flux in permafrost regions and implicitly or explicitly included in the model, and can be referred to in subsections of the Methods text. These refer to: (a) Biomass generation; (b) DOC generation and leaching; (c) Throughfall and its DOC; (d) Hydrological mobilisation of soil DOC; (e) Soil flooding; (f) Landscape routing of water and carbon; (g)

Infiltration and topography; (h) Floodplain representation; (i) Oceanic outflow; (j) Dissolved carbon export and riverine atmospheric evasion; (k) Turbation and soil carbon with depth (e.g. (Hugelius et al., 2013; Tarnocai et al., 2009), (Koven et al., 2015)); (l) Adsorption; (m) Priming.

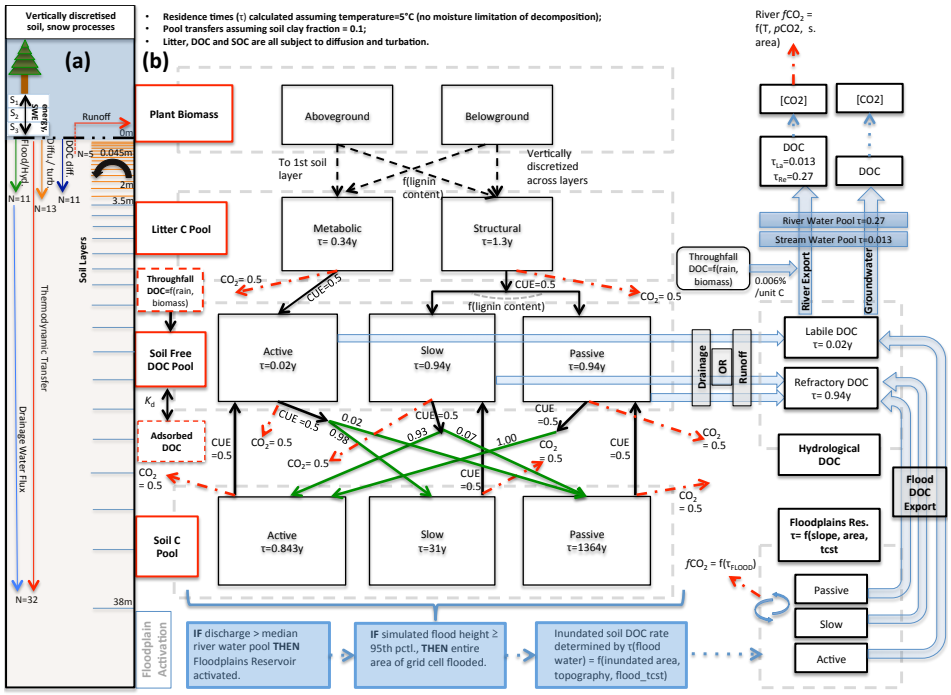

Figure 2 :Carbon and water flux map for core DOC elements in model structure relating to DOC transport and transformation. **(a)** Summary of the differing extent of vertical discretisation of soil and snow for different processes calculated in the model. Discretisation occurs along 32 layers whose thickness increases geometrically from 0-38m. N refers to the number of layers, SWE=snow water equivalent, S_n = Snow layer n. Orange layers indicate the depth to which diffusive carbon (turbation) fluxes occur. **(b)** Conceptual map of the production, transfer and transformation of carbon in its vertical and lateral (i.e., hydrological) flux as calculated in the model. Red boxes indicate meta-reservoirs of carbon, black boxes the actual pools as they exist in the model. Black arrows indicate carbon fluxes between pools, dashed red arrows give carbon loss as CO_2, green arrows highlight the fractional distribution of DOC to SOC (no carbon loss incurred in this transfer), a feature of this model. For a given temperature (5°C) and soil clay fraction, the fractional fluxes between pools are given for each flux, while residence times for each pool (τ) are in each box. The association of carbon dynamics with the hydrological module are shown by the blue arrows. Blue coloured boxes illustrate the statistical sequence which activates the boolean floodplains module. Note that for

readability, the generation and lateral flux of dissolved CO_2 is omitted from this diagram, but is described at length in the Methods section.

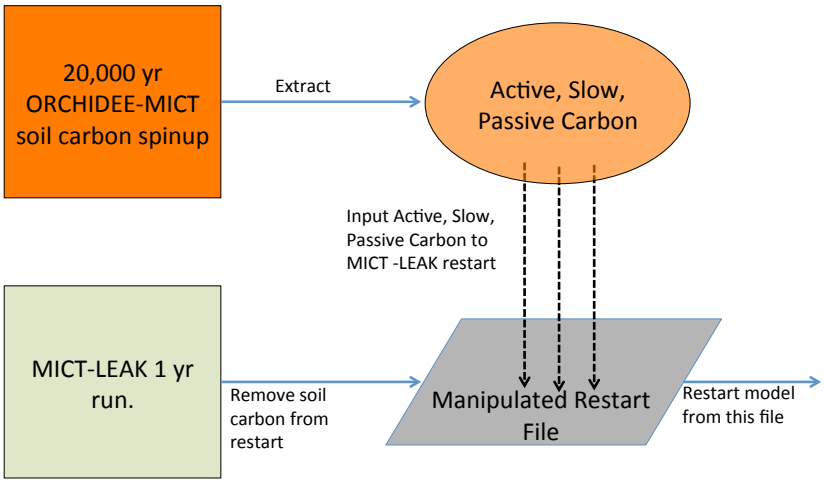

Figure 3: Flow diagram illustrating the step-wise stages required to implement the model's soil carbon stock prior to conducting transient, historical simulations.